NASA TECHNICAL NOTE

NASA TN D-6697

NASA TN D-6697

EXPERIMENTAL STUDY OF FLOW DISTRIBUTION AND PRESSURE LOSS WITH CIRCUMFERENTIAL INLET AND OUTLET MANIFOLDS

by Ralph T. Dittrich

Lewis Research Center
Cleveland, Ohio 44135

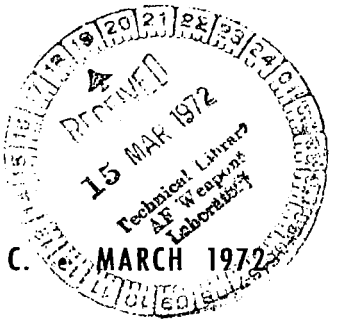

NATIONAL AERONAUTICS AND SPACE ADMINISTRATION • WASHINGTON, D. C. • MARCH 1972

1. Report No.	2. Government Accession No.	3. Recipient's Catalog No.
NASA TN D-6697		

4. Title and Subtitle	5. Report Date
EXPERIMENTAL STUDY OF FLOW DISTRIBUTION AND PRESSURE LOSS WITH CIRCUMFERENTIAL INLET AND OUTLET MANIFOLDS	March 1972
	6. Performing Organization Code

7. Author(s)	8. Performing Organization Report No.
Ralph T. Dittrich	E-6619
	10. Work Unit No. 112-27

9. Performing Organization Name and Address	11. Contract or Grant No.
Lewis Research Center National Aeronautics and Space Administration Cleveland, Ohio 44135	
	13. Type of Report and Period Covered
12. Sponsoring Agency Name and Address	Technical Note
National Aeronautics and Space Administration Washington, D. C. 20546	14. Sponsoring Agency Code

15. Supplementary Notes

16. Abstract

Water flow tests with circumferential inlet and outlet manifolds were conducted to determine factors affecting fluid distribution and pressure losses. Various orifice sizes and manifold geometries were tested over a range of flow velocities. With inlet manifolds, flow distribution was related directly to orifice discharge coefficients. A correlation indicated that nonuniform distribution resulted when the velocity head ratio at the orifice was not in the range of constant discharge coefficient. With outlet manifolds, nonuniform flow was related to static pressure variations along the manifold. Outlet manifolds had appreciably greater pressure losses than comparable inlet manifolds.

17. Key Words (Suggested by Author(s))

Manifold design; Circumferential manifold; Curved manifold; Inlet and outlet manifold; Manifold flow distribution; Manifold pressure losses; Manifold pressure distribution; Orifice discharge coefficients; Tangential manifold; Radial manifold; Orifice pressure loss

18. Distribution Statement

Unclassified - unlimited

19. Security Classif. (of this report)	20. Security Classif. (of this page)	21. No. of Pages	22. Price*
Unclassified	Unclassified	53	$3.00

* For sale by the National Technical Information Service, Springfield, Virginia 22151

EXPERIMENTAL STUDY OF FLOW DISTRIBUTION AND PRESSURE LOSS WITH CIRCUMFERENTIAL INLET AND OUTLET MANIFOLDS

by Ralph T. Dittrich

Lewis Research Center

SUMMARY

An experimental investigation was undertaken to determine factors affecting fluid flow distribution and pressure loss in circumferential manifolds. Water flow tests were conducted with both inlet and outlet manifolds surrounding a 15.1-centimeter-diameter simulated liquid-metal-boiler shell. Data were obtained over a range of flow velocities with each of six different orifice areas and three different manifold geometries.

With inlet manifolds having negligible friction loss, the flow distribution was related directly to orifice discharge coefficients. A correlation of orifice discharge coefficients with orifice-to-manifold velocity head ratios indicated that for a range of flow conditions the discharge coefficients were relatively constant. A nonuniform flow distribution resulted when velocity head ratios were not in the range of constant discharge coefficients.

With outlet manifolds, orifice flow is related to manifold local static pressure. Variations in static pressure along the manifold result in nonuniform flow distribution. Orifice flow is a minimum at the orifices located farthest from the manifold outlet connection. The static pressure variations result from combined effects of changes of local mass flow rate and losses caused by jet penetration and mixing. The relative magnitude of the pressure variation diminishes with an increase in orifice pressure drop (a decrease in orifice area).

Pressure losses with outlet manifolds were appreciably greater than with comparable inlet manifolds. With both inlet and outlet manifolds, the tangential type of manifold connection had lower total pressure loss than did the radial type.

INTRODUCTION

Knowledge of factors affecting fluid flow distribution and pressure losses in circumferential manifolds is necessary to the development of Rankine cycle liquid-metal boilers

for space electric powerplants. Boilers of the multiple-tube-in-shell type with fluid flow parallel to the tube axis have curved manifolds (as shown in the sketch) that distrib-

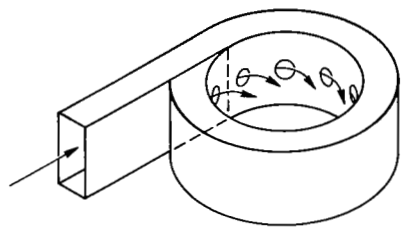

Circumferential manifold with tangential entry

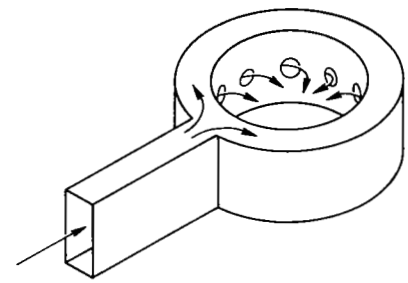

Circumferential manifold with radial entry

ute and collect, circumferentially, shell-side flow at the inlet and outlet ends, respectively, of the boiler shell. Compactness in design and efficiency in boiler performance require effective control of flow distribution within the boiler shell. A procedure for obtaining uniform radial distribution of flow at the ends of the tube bundle is presented in reference 1. A prerequisite for uniform radial distribution, however, is a uniform circumferential distribution at both inlet and outlet manifolds.

Pertinent factors affecting flow distribution include (1) discharge coefficients of orifices in inner walls of curved manifolds, (2) area ratio of orifice to manifold, (3) manifold geometry, and (4) friction and orifice throttling pressure losses. No comprehensive experimental results or relevant parameters are available to be of use for design purposes. Thus, the present experimental investigation was undertaken to evaluate these factors and to identify others of significance.

This introduction to a discussion of curved manifold flow will use a straight manifold as a reference model Recommended practice for the design of straight manifolds (ref. 2) is that the area ratio (ratio of sum of areas of all openings to the cross-sectional area of the manifold) should not exceed unity for moderate manifold lengths. Other than the visual observation of results, no basis for derivation of the ratio is indicated. Furthermore, in calculations of flow distribution (refs. 2 and 3), the discharge coefficient of a given orifice geometry was assumed constant for all openings in a given manifold. That the discharge coefficient of a given orifice can vary appreciably is shown in references 4 and 5. Discharge coefficients of orifices in walls of straight ducts were shown to vary from 0.0 to approximately 0.60 for thin wall orifices (ref. 4) and from 0.0 to a maximum of 0.85 for orifices in thick walls (ref. 5). The main factors affecting these discharge coefficients were reported to be approach velocity and the static pressure difference across the orifice.

Discharge coefficients evaluated for orifices in walls of straight ducts, however, may not be applicable to curved ducts because of the momentum and centrifugal forces present that affect the symmetry of both the velocity and pressure patterns within the duct. Profile measurements taken in the plane of curvature of square shaped elbows (ref. 6) indicate that, although both the total and static pressures were lowest, the velocity was highest in the region near the inner wall of the elbow. The portion of the flow having the higher total energy is directed by centrifugal force toward the outer wall of the curved channel, thereby displacing flow of lower total energy toward the inner wall. This action introduces a secondary flow pattern and creates a total pressure gradient between the inner and outer walls. This pressure gradient, however, is not readily calculated (ref. 7). In curved manifolds there are, in addition to the previously mentioned radial variations in pressure and velocity, the longitudinal variations due to local branch flow and to friction. With manifolds of constant cross-sectional area the static pressure increases in the direction of flow in inlet manifolds and decreases in the direction of flow in outlet manifolds. Also, discharge coefficients of orifices in outlet manifolds may differ from those for inlet manifolds. Furthermore, a knowledge of the magnitude of fluid friction losses and of the relation of orifice throttling pressure losses to flow distribution is essential to the design for maximum hydraulic efficiency.

Water flow tests were conducted with circumferential manifolds of rectangular cross section surrounding a 15.1-centimeter-diameter simulated boiler shell. The given diameter approximated that of a prototype boiler. The simulated shell was divided into six equal and isolated sectors, each sector having one of the six equal size orifices. Variables in manifold geometry include the radially and the tangentially oriented connection with system piping. By reversal of flow direction through the test section the function of the manifold was changed from an inlet to an outlet manifold. Flow distribution, discharge coefficient, and pressure loss data were obtained with six different orifice sizes from 1.59 to 3.19 centimeters in diameter for manifold velocities from approximately 0.0 to 2.1 meters per second.

The data are presented in tables and in figures to illustrate the trends. Discharge coefficients are correlated with a flow parameter as in reference 4. The data should be applicable to the design of circumferential manifolds for the prototype boiler as well as other types of heat exchangers of similar size.

SYMBOLS

A flow cross-sectional area, m^2

C_d discharge coefficient, ratio of measured to theoretical flow rate, dimensionless

K pressure loss coefficient, $\Delta P/q_a$, referred to dynamic pressure at reference station (a), dimensionless

P total pressure, N/m^2

p static pressure, N/m^2

q_a dynamic pressure at reference station (a), N/m^2

V fluid mass velocity, m/sec

W mass flow rate, kg/sec

ρ fluid density, kg/m^3

Subscripts:

a reference station

d straight duct

j orifice jet flow

m manifold

o orifice

s sector

t theoretical

APPARATUS

A schematic of the apparatus used for the inlet manifold tests is shown in figure 1(a). For the outlet manifold tests the components were rearranged (fig. 1(b)) so as to reverse the direction of flow through the test section. Flow through the system was recirculated by means of a centrifugal pump, while flow rate and distribution were controlled by either gate or ball valves. The 2.9-meter-long duct of rectangular cross section functioned as a flow conditioner with inlet manifolds.

Boiler Shell

The geometry and size of the test section were based on a conceptual design of a prototype boiler shell and manifold. Two simulated boiler shells were fabricated; One boiler shell was retained for reproducibility tests, while in the other boiler shell the orifices were enlarged to the next size in the series of tests. The interior of the boiler

shell (14.6 cm) was divided into six equal-sized isolated sectors, each sector having one circular orifice in the curved wall facing the surrounding manifold (fig. 2). The outlet at the lower end of each sector was connected with a branch flowmeter (fig. 1).

To simplify data comparison among the six orifices of a given test series, the orifice sizes were carefully machined so that the maximum variation in area among the six orifices of any series was approximately 0.25 percent. Six different series of orifice sizes were tested with inlet manifolds and five with outlet manifolds. The average orifice sizes and designations are given in table I.

TABLE I. - ORIFICE SIZES TESTED

Orifice designation	Average orifice diameter, cm	Average orifice area, cm^2
A	1.589	1.98
B	1.907	2.86
C	2.285	4.10
D	2.543	5.08
E	2.860	6.42
F	3.175	7.92

Manifolds

The test manifolds were formed by the circumferential channel surrounding the series of six orifices that are equally spaced around the periphery of the boiler shell. Two manifolds differing in cross-sectional area and flow pattern are shown in figure 2. The manifolds are identified as tangential or radial by the flow pattern produced with the connection to the loop piping. These manifolds, which were interchangeable on either of the two boiler shells, were designed to represent extremes in manifold geometry that could influence pressure loss, flow distribution, or discharge coefficient values. The tangent duct has a rectangular cross section equal to that of the manifold (4.12 by 14.28 cm; area, 58.83 cm^2). The walls of the rectangular duct were continuous to the line of tangency in the curved manifold, thereby limiting manifold flow to less than one revolution. On assembly, the inner duct wall was always made tangent to the boiler shell at the edge of the neighboring orifice. The manifold with the radial connection had a cross-sectional area equal to one-half (2.06 by 14.28 cm; area, 29.42 cm^2) that of the connecting duct. This radial manifold was assembled to the boiler shell in either of two positions. In position 1 the straight duct centerline was located midway between a pair of orifices; in position 2 the duct centerline coincided with that of one of the orifices. Depending on the

direction of fluid flow (fig. 1), the test section functioned as either an inlet or outlet configuration. Thus, six manifold configurations differing in either geometry or function were tested and are listed in table II.

One important parameter in this study is the ratio of the sum of orifice areas within the manifold to the cross-sectional area of the manifold. This term will be identified as "area ratio" in this report. With radial manifolds each half is considered a separate manifold. For configurations with "inline" orifices (RIM-2, ROM-2) each radial manifold was considered to contain only two and one-half orifices. Table III lists the area ratios for the various orifice-manifold combinations tested.

TABLE II. - DESIGNATIONS OF MANIFOLDS TESTED

Designation	Description
TIM	Tangential inlet manifold
RIM-1	Radial inlet manifold, duct between orifices
RIM-2	Radial inlet manifold, duct inline with orifice
TOM	Tantential outlet manifold
ROM-1	Radial outlet manifold, duct between orifices
ROM-2	Radial outlet manifold, duct inline with orifice

TABLE III. - AREA RATIOS OF VARIOUS ORIFICE-MANIFOLD COMBINATIONS

Orifice designation	TIM, RIM-1 TOM, ROM-1	RIM-2 ROM-2
	Area ratio	
A	0.20	0.17
B	.29	.24
C	.42	.35
D	.52	.43
E	.66	.55
F	.81	.67

Instrumentation

The water flow rates through each of the six branches as well as the total combined flow were measured with turbine-type flowmeters having a rated precision of 0.5 percent. The meters were calibrated before and after the test series. Flowmeter turbine frequencies were registered with an electronic counter.

With the use of water as the test fluid the absolute pressures were of no consequence, only pressure differences between designated points were considered. Pressure differences were measured by means of common well manometers. The manometers contained an indicating fluid that had a nominal specific gravity of 1.75 in contact with water, the pressure transmitting fluid. All pressure levels reported herein are pressure differences referenced to the static pressure at station a (fig. 1(a)), which is located in the rectangular duct. Static pressure taps were located in the floor of the manifolds directly below each orifice and in the ceiling of each sector. The pressures measured in the floor of the manifolds were considered representative of the channel static pressure at each location. The pressure taps in the sector ceilings were designed to

minimize gas entrainment. Circulating water temperatures were measured by means of a glass thermometer immersed in the flowing stream.

PROCEDURE

Fluid flow rate and pressure drop data were obtained with each of the six manifold configurations for each orifice size investigated. Each configuration was tested at several fluid flow velocities within the range of 0.3 to 2.1 meters per second as measured at the reference station a.

In order that the data obtained with the six orifices in a given test be comparable it was necessary to equalize pressures among the six boiler sectors. This was attempted by careful adjustment of each branch flow rate by means of manually operated ball valves located in the branch flowmeter lines (fig. 1(a)). However, some instability among the branch flows persisted at all operating conditions. Because of this instability, the flowmeter signals were averaged for 10-second periods, and three successive agreements in flowmeter recordings were the criteria for acceptable data. Also, the six sector pressures, which were recorded by photographing the manometer panels, were averaged arithmetically for calculation purposes.

Pumping recirculating water caused some separation of dissolved gases from the water. The effects of these gases on test results were minimized by partially degassing the fluid before testing. The fluid was pumped against relatively high back pressures until a temperature rise of approximately 40° C was obtained. Testing began after cooling the system to room temperature and venting the separated gases.

To determine reproducibility the three inlet manifold configurations with size D orifices (see table I) were tested at the beginning and again near the conclusion of the test program.

The experimental data obtained from the tests of the inlet and outlet manifolds are tabulated in table V(a) and (b), respectively, at the end of the report.

CALCULATIONS

Pressure Loss

Total pressure losses due to wall friction and turbulence within the duct and manifold and to throttling at the orifices are presented in terms of a pressure loss coefficient K referred to the velocity head at station a:

$$K = \frac{\Delta P}{\rho \frac{V_a^2}{2}} \tag{1}$$

Straight duct. - The total pressure loss along the flow conditioner duct is given by

$$\Delta P_{d-a} = (P_d - P_a) = \left(p_d + \rho \frac{V_d^2}{2}\right) - \left(p_a + \rho \frac{V_a^2}{2}\right) = (p_d - p_a) \tag{2}$$

since

$$\left(\rho \frac{V_d^2}{2}\right) = \left(\rho \frac{V_a^2}{2}\right) \tag{3}$$

for incompressible flow in a duct of constant cross-sectional area.

Inlet manifold. - The pressure losses in inlet manifolds were computed using the following equation:

$$\Delta P_{a-m} = (P_a - P_m) = \left(p_a + \rho \frac{V_a^2}{2}\right) - \left(p_m + \rho \frac{V_m^2}{2}\right) \tag{4}$$

where p_a is the reference static pressure at station a and p_m is taken at the floor tap in the manifold directly below the given orifice. The computation of the velocity term V_m with inlet manifolds was based on the manifold mass flow rate approaching the given station.

An overall total pressure loss was calculated that includes the previously mentioned manifold losses with losses due to orifice throttling:

$$\Delta P_{a-s} = (P_a - P_s) = \left(p_a + \rho \frac{V_a^2}{2}\right) - (p_s) \tag{5}$$

Within the sector p_s was considered equal to P_s since the orifice discharged into a relatively large passage and the flow was required to turn at right angles therein (ref. 9).

Outlet manifold. - Equations (2) and (4) were used with outlet manifold data after rearranging the subscripts to reflect the reversal in direction of flow and basing the velocity term V_m on the manifold mass flow rate leaving the given station.

Overall total pressure losses with outlet manifolds were based on the difference in total pressures between the boiler sectors and the reference station a:

$$\Delta P_{s-a} = (P_s - P_a) = (P_s) - \left(p_a + \rho \frac{V_a^2}{2}\right) \tag{6}$$

With reversed flow through the test section the pressures taken at the ceiling of each sector were considered a stagnation or total pressure.

Distribution

Ideal flow is defined as equal flow distribution among the six orifices of a given test. Percent deviation from ideal flow was computed as follows:

$$\text{Percent deviation} = \frac{W_j - \frac{W_a}{6}}{\frac{W_a}{6}} \times 100 = \frac{600\ W_j}{W_a} - 100 \tag{7}$$

Because the variation among orifice sizes was negligibly small, the areas of each of the six orifices in a given test were considered equal in all computations.

Discharge Coefficients

The orifice discharge coefficient C_d with curved manifolds was calculated as the ratio of measured to theoretical mass flow rates through the orifice:

$$C_d = \frac{W_j}{W_t} \tag{8}$$

where, for incompressible flow,

$$W_t = A_o \rho_j V_j = A_o \sqrt{2\rho_j (P_j - p_j)} \tag{9}$$

Inlet manifolds. - Applied to inlet manifolds the pressure drop term $(P_j - p_j)$ becomes $(P_m - p_s)$. The determination of a local total pressure by the usual method

$$P_m = \left(p_m + \rho \frac{V_m^2}{2} \right) \tag{10}$$

was found to be questionable at some stations in the curved manifolds because of flow irregularities at the inlets. The method used in the present investigation consisted of adjusting the reference total pressure P_a at station a for friction loss up to the local orifice station. However, since the measured variation in friction loss to the various stations was relatively small, a single value determined at midlength was used for all orifice stations. A mean value of the pressure loss coefficient K_{a-m_o} was evaluated from friction data for each configuration at a station approximately 90^o into the curved

TABLE IV. - PRESSURE LOSS COEFFICIENTS OF VARIOUS CONFIGURATIONS

Inlet manifold configuration	Pressure loss coefficient, K, dimensionless
TIM	0.08
RIM-1	.30
RIM-2	.38
At inline orifice	.00

manifold as given in table IV. The net pressure drop across the orifice was then determined as follows:

$$\left.\begin{aligned}(P_m - p_s) &= \left(p_a + \rho \frac{V_a^2}{2}\right) - K\left(\rho \frac{V_a^2}{2}\right) - p_s \\ &= (p_a - p_s) + (1 - K)\, \rho \frac{V_a^2}{2}\end{aligned}\right\} \tag{11}$$

The arithmetic average of the pressures recorded of the six sectors was used as the orifice discharge pressure p_s. Because of the unstable and sometimes oscillating flows among the six sectors, equal pressures could not be maintained by adjustment of flow rates. The arithmetic average of the six pressures was considered more representative of the effective pressure than the recorded individual instantaneous pressures.

Discharge coefficients of orifices in inlet manifolds are correlated with a flow parameter that is defined as the ratio of the velocity head of the orifice jet to the velocity head of the manifold flow approaching the orifice:

$$\text{Velocity head ratio} = \frac{P_m - p_s}{P_m - p_m} \tag{12}$$

This ratio is similar to that used in reference 4 to correlate discharge coefficients of wall orifices in straight ducts.

Outlet manifolds. - Theoretical mass flow rates through orifices in outlet manifolds were determined with equation (9) after changing the subscripts of the pressure drop term to read $P_s - p_m$. With the direction of orifice flow into the manifold the pressure in the ceiling of the sectors was considered a stagnation or total pressure P_s. As with the inlet manifold calculations, the arithmetic average pressure of the six sectors was used. A single-valued manifold static pressure p_m, however, could not be used with outlet manifolds because of the variance in pressures along the manifold. Therefore, discharge coefficients of orifices in outlet manifolds are based on individual pressure drops between sector total pressure P_s and the local manifold static pressure p_m as measured at midradius in the floor of the manifold directly below the subject orifice.

RESULTS

Fluid flow and pressure data were obtained with six different manifold configurations for a range of orifice sizes. These data were the basis for determining manifold pres-

sure maps, friction pressure losses, orifice throttling pressure losses, flow distribution, and orifice discharge coefficients for both inlet and outlet manifolds.

Manifold Pressure Maps

Typical pressure distribution maps of inlet and outlet manifolds showing effects of different flow patterns due to manifold geometry and orifice location are presented in figures 3 and 4. In these figures the pressures at various stations are given relative to the pressure at reference station a and are shown spaced according to manifold centerline distances from station a. The flow direction is given from left to right.

Inlet manifolds. - The pressures obtained with inlet manifolds showed no effects due to orifice size or orifice pressure drop; therefore, the data presented are considered typical of other sizes and were selected to include combinations that cover the range of orifice sizes and pressure drops investigated. Inlet manifold total pressures are derived by adding local approach flow velocity head to the local measured static pressure. The relatively high total pressure shown at station 4 (fig. 3(a)) resulted from the increased static pressure measured at that station. This high static pressure is believed due to pressure disturbance created by curved channel flow and found to extend upstream of the curved channels (ref. 7). The dashed lines indicate the average values of P_m and p_s used in flow calculations. The deviation of actual pressures from these average values is shown to be negligibly small relative to the indicated pressure drop across the orifice.

Figure 3(b) shows the pressure distribution in the radial inlet manifold (RIM-1) with size F orifices at a relatively low orifice pressure drop. Static pressure recovery is indicated at stations 1, 4, 5, and 6; however, the static pressures at stations 2 and 3 are shown to be exceptionally low. This low pressure is believed to be an effect of the sharp cornered turn of the flow at the radial inlet to the manifold. This relatively low static pressure would indicate an appreciable local increase in velocity due to stream contraction as it flows past the sharp corners (ref. 9). Therefore, no total pressure evaluation at stations 2 and 3 of model RIM-1 manifolds was attempted.

The radial manifold RIM-2 represented in figure 3(c) featured size A orifices, high orifice pressure drop, and an orifice inline with the radial inlet duct. The relatively high static pressure shown at station 3 (the inline orifice) is apparently an effect of flow pattern at the tee connection on static pressure measurement. With inline orifices, such as at station 3, calculations of mass flow rate are based on the reference total pressure P_a.

Outlet manifolds. - The accuracy of outlet manifold static pressures is important because pressure losses and theoretical mass flow rates are based on them. The static

pressures measured at the closed ends of manifolds are considered valid because of the low flow disturbance and velocity levels that exist in this area. However, the variation in static pressure along the manifold is shown (fig. 4(a)) to be nonuniform while some total pressures are shown to increase in the direction of flow. Similar pressure profiles were obtained with all TOM configurations. This rise in total pressure would indicate that measured static pressures at the affected stations do not represent true static pressures. It is not known whether this discrepancy is due to secondary flow patterns created by the orifice jet (ref. 8), by curved channel flow (ref. 7), or by the proximity of the pressure tap to the orifice. The extent of this effect on static pressures in the narrower ROM models is masked by the additional pressure losses caused by the tee connection. In the absence of an analysis the measured static pressures are used in the calculations. In most cases the effect of this discrepancy on results is relatively small.

Manifold Pressure Losses

Typical pressure loss data for the six manifold configurations and the flow conditioner duct are presented in figures 5 and 6 in terms of the pressure loss coefficient K. The pressure losses considered here are those due to wall friction, stream turning, mixing, and turbulence; the losses do not include the pressure drop across the orifice. With the flow direction from left to right in the figures the various stations are spaced to scale relative to station a. A straight line connecting the pressure loss data of the flow conditioner duct is extended to the manifold stations for comparison purposes. This extrapolation is considered to represent the pressure loss gradient due to wall friction only. With outlet manifold configurations this line is shown (fig. 6) to favor the data at stations b and c of the straight duct. This may be justified by the premise that pressure losses resulting from flow disturbances may not be confined to the immediate area of the disturbance. It was observed with elbows (ref. 6) that pressure losses due to curved flow phenomena are not limited to the elbow but continue downstream until the flow pattern returns to normal pipe flow. Thus, the pressure losses measured at the downstream stations of the straight duct were considered more representative of loss due to wall friction only than those losses at the upstream stations. A comparison in figures 6(a) and (b) indicates that additional pressure losses are occurring in the region of stations a and A. The disagreement shown in figure 6(c) may be due to the proximity of stations a and A to the discharging jet from the inline orifice affecting pressure measurements.

Overall Total Pressure Loss

The overall total pressure loss coefficient obtained with both inlet and outlet manifolds is plotted in figures 7 and 8 in terms of the total area of the six orifices in a given test. The overall total pressure loss for inlet manifolds represents the difference in total pressure between the reference station a and the boiler sectors. Manifold friction loss data are included in the figures for comparison. The difference between the overall total pressure loss coefficient and the manifold loss is the orifice pressure loss coefficient. The plotted points indicate the arithmetic average of the range of data obtained with the given configuration. Reproducibility of inlet manifold data is indicated by the tailed symbol for the 30.5-square-centimeter orifice size.

Flow Distribution

Flow distribution data obtained with the six manifold configurations are shown in figures 9 and 10. Six orifice sizes were tested with inlet manifolds and five with outlet manifolds. The data are presented in terms of percent deviation at the various orifices from an ideal or uniform distribution. The data points shown are average values of several (4 to 10) runs covering a range of velocities from about 0 to 2.1 meters per second.

Discharge Coefficients

Variation in discharge coefficients with orifice size and location in each of the six manifold configurations is shown in figures 11 and 12. Each data point represents an average of several runs made at different flow rates. The straight lines shown in the figures are intended only to connect like symbols and not to indicate trends.

Inlet manifolds. - The pattern of discharge coefficients with inlet manifolds is similar to that shown for the flow distribution data in figure 9. This necessarily follows since the differences in measured flow rate for each orifice are the only variable affecting the calculations of discharge coefficients for a given test run.

Outlet manifolds. - With outlet manifolds, the discharge coefficients of the six orifices in a given test run are a function of flow rate and pressure drop, both of which may vary. Therefore, the pattern of discharge coefficients in figure 12 may show little relation to the flow distribution patterns of comparable configurations in figure 10.

Correlation of discharge coefficients. - Discharge coefficients for all orifices tested with inlet manifolds are plotted against the velocity head ratio in figures 13 and 14. Included for comparison is a dashed line curve from reference 4 representing

the correlation of discharge coefficients for orifices in walls of straight ducts.

The data points of all orifice stations excepting those at station 4 of the tangential inlet manifold TIM are shown in figure 13(a). The data of station 4 are not comparable to those at other stations because a transition between the straight and curved channel flow patterns is considered to be developing in that area. The data of station 4 are shown in figure 13(b).

The data of both radial inlet manifolds RIM-1 and RIM-2 are shown in figure 14. Included in this figure are the straight duct correlating curve of reference 4 and the transition and curved manifold flow correlating curves from figure 13. The data of stations 5 and 6 (fig. 14(a)) and station 6 (fig. 14(b)) show a trend of reduced orifice discharge coefficients with an increase in orifice diameter. This variation in discharge coefficient with orifice size is believed to be an effect of manifold width relative to orifice diameter (ref. 4) (manifold width measured perpendicular to plane of orifice). This effect was not evident with the tangential manifold data (fig. 13(a)) where manifold width was greater than orifice diameter.

Discharge coefficients obtained with outlet manifolds are not subject to correlation as with inlet manifolds; however, they are shown plotted against orifice diameters in figure 15.

Reproducibility

Check runs made with size D orifices and the three inlet manifold arrangements are indicated by the tailed symbols in figures 7, 9, and 11. The data of these runs deviate from the original data by less than 5 percent in pressure losses, 2 percentage points in deviation from ideal flow distribution, and 0.025 unit in discharge coefficients.

DISCUSSION

In this discussion, an attempt is made by analyzing the data to determine factors affecting manifold pressure loss and flow distribution and to develop procedures for design of efficient prototype manifolds.

Manifold Pressure Maps

Inlet manifolds. - The data obtained with the three inlet manifolds (fig. 3) show a gradual increase, in direction of flow, in manifold static pressure due to local velocity head recovery, while manifold total pressures are approximately constant at all stations. For inlet manifolds in which friction losses are relatively small, the use of

manifold total pressure simplifies the computations. Thus, in both the derivation and application of discharge coefficients for inlet manifolds, a single pressure drop term ($P_m - p_s$) may suffice for all orifices. For improved accuracy an average pressure P_m may be used as in the present case. The deviation of the individual pressures (P_m and p_s) from their respective average values is shown (fig. 3) to be negligibly small relative to the magnitude of the orifice pressure drop.

Outlet manifolds. - The indicated static pressure gradient in outlet manifolds is greater than that due only to flow acceleration, especially with radial manifolds having the narrow flow passage. This increased slope would indicate significant pressure losses due to turbulent mixing and friction at the jets and that a decrease in manifold width intensifies this loss. The magnitude of this static pressure variation precluded the averaging of these pressures for flow calculations.

Manifold Pressure Loss

Inlet manifolds. - A comparison of curved manifold pressure loss with that indicated by the friction pressure loss gradient (fig. 5(a)) shows that pressure losses with TIM models approximates that of an equivalent length of full flowing straight duct. A similar comparison in figures 5(b) and (c) indicates that radial manifolds have additional pressure losses. These are due mainly to the dividing flow and sharp corner turning at the tee connection. No trend in pressure loss coefficient K due to orifice size or mass flow rate could be detected within the ranges investigated.

Outlet manifolds. - Pressure loss coefficients obtained with the three outlet manifolds (fig. 6) are shown to be significantly greater (up to six times greater) than with similar inlet manifolds (fig. 5). Also, with outlet manifolds a relatively small effect of orifice size was noted; decreasing the orifice size increased the manifold pressure loss (fig. 8). Qualitatively, both trends are verified (refs. 10 and 11) by tests conducted with straight round pipes. The increased pressure loss is due to the relatively high velocity orifice jets penetrating the outlet manifold stream. The jets obstruct part of the cross-flow area (ref. 8), create a high level of turbulence in turning, and mix with the low velocity stream. Since jet velocity is many times greater (in the present tests) than manifold velocity, the jet flow has a controlling influence on the resulting flow pattern.

A comparison (figs. 5 and 6) favors the tangential manifold for low pressure losses in both the inlet and outlet versions. However, modified radial manifold designs incorporating efficient diffusers, rounded corners, where essential, and a relatively large cross-sectional area with a low aspect ratio may be competitive with the tangential type.

Overall Total Pressure Loss

The relative magnitude of the orifice or throttling pressure loss to that of manifold friction is shown in figures 7 and 8. With each of the inlet manifolds tested, the combined pressure loss coefficient K decreased from approximately 70 to 6 with an increase in orifice total area from 11.9 to 47.5 square centimeters. The manifold friction loss coefficient is shown to be approximately constant at a value of less than 0.4 over the same orifice area range. Comparable outlet manifolds show a somewhat lower (10 to 29 percent) combined loss but with manifold friction accounting for up to 44 percent of the combined loss.

Although high levels of orifice pressure drop within the range investigated tended to reduce instability somewhat, there was no indication that the level of orifice pressure drop, in itself, affected flow distribution.

Flow Distribution

Inlet manifolds. - With all configurations tested the percent deviation from ideal flow was a maximum with the largest of the six orifice sizes tested and decreased with a decrease in orifice size or "area ratio". For inlet manifolds (fig. 9) this deviation was negative for the larger orifices located within approximately 60° of the inlet connection except for the inline orifice (fig. 9(c)) where the deviation was positive. Large orifices located roughly beyond 60° from the connection had increasingly greater positive deviations. This nonuniform distribution, however, is not attributed directly to orifice size, but to a variation in orifice discharge coefficients that will be discussed later.

Outlet manifolds. - Flow distribution patterns obtained with outlet manifolds (fig. 10) are in the reverse order of those shown for inlet manifolds; that is, deviations are positive and increase with an increase in orifice size for orifices located within 60° of the outlet connection and are increasingly negative for orifices located beyond the 60° location. The inline orifices which are considered outside the manifold have but a small deviation over the range of sizes tested.

With outlet manifolds the orifice flow is related to manifold local static pressure. Variations in this static pressure result in nonuniform flow distribution. Orifice flow is a minimum at locations farthest from the manifold outlet connection (fig. 10). The pressure variations (fig. 4) result from combined effects of local velocity changes and an abnormal friction factor due to orifice jet penetration blocking manifold flow. The magnitude of this manifold pressure variation remained approximately constant for a range of orifice sizes over which orifice pressure drops varied by a factor of more than

six (fig. 8). Thus, the relative magnitude of manifold pressure variations diminished with an increase in orifice pressure drop (a decrease in orifice area).

Flow distributions within 4 percent of ideal were obtained with all three manifold types having an orifice area of 24.6 square centimeters or less (fig. 10). With an orifice area of 24.6 square centimeters the resulting orifice-to-manifold area ratios ($A_{o,total}/A_m$) are 0.42 for the TOM and ROM-1 configurations and 0.35 for the ROM-2 model. The corresponding net orifice pressure drop coefficients K varied within the range of approximately 11.9 to 14.0 for the three outlet manifold configurations (fig. 8).

Discharge Coefficients

Inlet manifolds. - Reference 4 correlated the discharge coefficients of single orifices located in the wall of a straight, rectangular duct with the following orifice-to-duct velocity head ratio:

$$\frac{P_d - p_j}{P_d - p_d} \cong \frac{P_m - p_s}{P_m - p_m} \cong \frac{\frac{1}{2}\rho V_j^2}{\frac{1}{2}\rho V_m^2} \tag{13}$$

where V_j is the orifice jet velocity and V_m the velocity in the manifold approaching the orifice. The correlation obtained by reference 4 is shown as the dashed curve in figure 13. Figure 13(a) plots the orifice discharge coefficients (fig. 11) of the tangential inlet manifold (TIM) for all orifice stations excepting station 4. As shown in figure 13(a), the discharge coefficients fall closely on the correlating curve of reference 4 at the higher values of the velocity head ratio. However, at the lower velocity head ratios the data exhibit lower values of the discharge coefficient than obtained with the straight duct. This deviation at the low velocity head ratios is believed to be an effect of the curved manifold flow, the deviation probably becoming less pronounced as the radius of the manifold increases. Figure 13(a) suggests than an orifice in a curved manifold requires for an equal flow rate a reduced manifold velocity head compared to that of a straight duct with an equal orifice velocity head.

The curved manifold orifice discharge coefficient data are correlated by the solid line in the figure. This correlation indicates that orifice discharge coefficients in curved manifolds are not a function of orifice diameter but rather a function of orifice-to manifold velocity head ratio (compare the discharge coefficients of orifice size F at station 5 (fig. 13(a)) with the same size orifices at downstream stations).

Figure 13(b) presents orifice discharge coefficients as functions of velocity head ratio for orifice station 4 of the same inlet manifold. The curve obtained from figure 13(a) for the other orifice stations is likewise shown in this figure. The data for orifice station 4 at low values of the velocity head ratio fall between the straight duct and the curved manifold data suggesting that the flow in the immediate vicinity of station 4 is in transition between linear and curved manifold flow. Again, at the higher values of the velocity head ratio, the data for station 4 tend to agree closely with the correlation obtained by reference 4. A line drawn through the data for orifice station 4 is shown in figure 13(b).

Figure 14 presents the orifice discharge coefficient data for the two radial inlet manifolds (RIM-1 and RIM-2) as a function of the orifice-to-manifold velocity head ratio. Curves corresponding to the straight duct correlation of reference 4 and the transition and curved manifold flow data of figure 13 are likewise shown in the figure. The radial manifold data are shown to agree well with the correlations. In particular, the solid data points of figure 14(a) for orifice stations 2 and 3 of the RIM-1 manifold fall along the transition flow curve obtained from figure 13(b). Evidently, the flow in proximity to these orifices was in transition even though stations 2 and 3 were located further downstream from the manifold inlet than station 4 of the tangential manifold. In figure 14(b), the orifice discharge coefficients for various sized orifices tested at station 6 of the RIM-2 manifold are plotted as solid data points. These coefficients are shown to fall progressively below the correlating line as the orifice diameter increases. Although less prominent, this phenomenon is also present in the data of figure 14(a) and is believed due to an effect on the discharge coefficients of the width of the manifold relative to the orifice diameter. A similar effect was observed by reference 4.

Examination of figures 9, 13, and 14 reveals that relatively uniform tangential and radial inlet manifold flow distribution is achieved when the discharge coefficients of a particular orifice series are equal, that is, on the flat portion of the correlating curves. Moreover, within a given orifice series, the orifice-to-manifold velocity head ratio is always a minimum at the first orifice and increases at subsequent orifices in the direction of flow. This is illustrated in figures 13 and 14 for the series A to F orifices. The increase of velocity head ratio along the manifold results from the decrease of manifold velocity due to branch (orifice) flows while the orifice jet velocities remain constant (eq. (13)). As a consequence, in designing a manifold similar to the ones tested, a value of the velocity head ratio for the first orifice should be selected to yield a discharge coefficient along the flat portion of the curve. This will insure that all the orifices of the manifold will have higher values of the velocity head ratio and the flow distribution will be relatively uniform. A minimum value of about 40 for the velocity head ratio of the first orifice is suggested by the data of figures 13 and 14 for the manifolds tested.

A total orifice-to-manifold area ratio may be determined from a knowledge of the required velocity head ratio at manifold entrance. From continuity, all the flow enter-

ing the manifold must discharge through the orifices; thus, the velocity head ratio (orifice jet velocity head to manifold entrance velocity head) at the entrance is also related to the total orifice-to-manifold area ratio as follows. For incompressible flow,

$$\sqrt{\frac{P_m - p_s}{P_m - p_m}} \cong \frac{V_j}{V_m} \cong \frac{A_m}{A_j} \cong \frac{A_m}{C_d A_o} \tag{14}$$

where A_m refers to manifold cross-sectional area, and A_j and $C_d A_o$ refer to total jet area.

Equation (14), in conjunction with the previously mentioned value of the first orifice velocity head ratio (40) and its corresponding discharge coefficient (0.57), can be employed to compute an approximate maximum value of the orifice-manifold area ratio for relatively uniform flow distribution:

$$\frac{A_m}{C_d A_o} \cong \sqrt{40} \tag{15a}$$

$$\frac{A_o}{A_m} \cong 0.28 \tag{15b}$$

This area ratio applies only to inlet manifolds of the type tested. Moreover, with radial type manifolds, the ratio does not include the area of an inline orifice which must be treated separately.

A method of applying the test results for inlet manifolds to the design of the prototype boiler-manifold is given in the appendix.

Outlet manifolds. - Although outlet manifold discharge coefficients are not a major factor in flow distribution, they are essential in sizing orifices and determining flow rates. The levels of discharge coefficient values obtained with outlet manifolds (fig. 12) are significantly greater than those obtained with inlet manifolds, and they tended to increase with an increase in orifice size (fig. 15), which is contrary to the trend shown with inlet manifolds. The increased level in discharge coefficient can be attributed to the difference in geometry between the two orifice surfaces. With the flow approaching the orifice from inside the shell the curvature of the shell simulates, in part, a converging inlet and thereby decreases the contraction of the discharge jet (ref. 5). The increased discharge coefficient with increase in orifice diameter may result from the increased slope of the shell at the sides of the orifice as orifice diameter was increased.

The discharge coefficients obtained with both radial manifolds are shown over the

range of orifice sizes (fig. 15) to be consistently higher in value than with the tangential manifold. However, the use of the discharge coefficients of the tangential manifold (fig. 15(a)) is preferred for design purposes because of the greater manifold dimension perpendicular to the plane of the orifice.

The application of the present results to the prototype boiler is discussed in the appendix.

SUMMARY OF RESULTS

In an experimental investigation of factors affecting fluid flow distribution and pressure losses in both inlet and outlet circumferential manifolds on a simulated 15.1-centimeter-diameter boiler shell the following results were obtained:

1. Orifice discharge coefficients of inlet manifolds were correlated with an orifice-to-manifold velocity head ratio. The discharge coefficients were relatively constant over a wide range of velocity head ratio values but decreased sharply in the lower range.

2. Inlet manifold flow distribution was found to be relatively uniform when the values of the discharge coefficients of all the orifices in a manifold were constant with velocity head ratio.

3. The orifice-to-manifold velocity head ratio was shown to be related to the orifice total area. Thus, flow distribution in inlet manifolds was related to orifice total area. For inlet manifolds of the type tested which have negligible friction losses, a ratio of orifice total area to manifold area of about 0.28 or less resulted in relatively uniform flow distribution.

4. Orifice diameter, by itself, did not affect discharge coefficients of inlet manifolds. However, large orifice diameters relative to the manifold width were shown to reduce the values of these coefficients.

5. Discharge coefficient values were significantly larger with outlet manifolds compared to inlet manifolds and increased with an increase orifice diameter. These were effects of the concave curvature of the orifice surface.

6. Total pressure loss and static pressure variations in outlet manifolds were appreciably greater than with comparable inlet manifolds.

7. Static pressure variation along outlet manifolds had a major effect on uniformity of flow distribution.

8. The relative effects of static pressure variations on flow distribution were reduced by using relatively high orifice pressure drop.

9. With both inlet and outlet manifolds, the tangential type of entry had lower total pressure losses than did the radial type.

Lewis Research Center,
National Aeronautics and Space Administration,
Cleveland, Ohio, November 22, 1971,
112-27.

APPENDIX - APPLICATION OF DATA

The pressure loss, flow distribution, and discharge coefficient data presented in this report may be applied to either an evaluation or design of curved inlet and outlet manifolds. Although the approach should be applicable to all sizes, the data are specifically related to circumferential manifolds having an inner wall diameter of approximately 15 centimeters. Boiler design may depend on parameters other than ideal manifold flow and therefore may vary to suit specific applications. A specific design may be the result of a compromise between the additional size, cost or weight of manifold and fluid required for ideal flow distribution at low pressure loss and the increased initial and operating costs of higher fluid pumping losses required with smaller flow passages.

INLET MANIFOLDS

The present method for obtaining uniform flow distribution with inlet manifolds assumes a constant value of discharge coefficient for all orifices and a negligible manifold friction loss. The first consideration is the orifice-to-manifold area ratio. For the subject boiler diameter this ratio has been evaluated (eq. (15b)):

$$\frac{A_{o,total}}{A_m} = 0.28 \tag{A1}$$

For a given mass flow rate and either a given or an assumed orifice pressure drop the orifice total area is determined by using

$$A_{o,total} = \frac{W}{(C_d)\sqrt{\rho 2(P_m - p_s)}} \tag{A2}$$

The value of C_d was previously selected as 0.57. With divided flow, as in radial manifolds, the given mass flow rate W is reduced by one-half. Since inlet manifold orifice size does not affect discharge coefficients, the orifice total area A_o may be divided equally among any number of orifices as indicated by other boiler design considerations. The manifold cross-sectional area A_m is determined from equation (A1) and the previously determined value of A_o. If the resulting manifold size is considered excessive, a new A_o is determined on the basis of an increased orifice pressure drop $(P_m - p_s)$.

Although tangential manifolds may have advantages not found in radial types, for a given orifice-to-manifold area ratio the tangential requires twice the cross-sectional

area. One consideration in manifold cross-sectional shape is that the dimension perpendicular to the orifice surface should be greater than orifice diameter to eliminate an effect of this dimension on reducing orifice discharge coefficients (fig. 14 and ref. 4).

OUTLET MANIFOLDS

Although an ideal distribution with outlet manifolds cannot theoretically be obtained with equal sized orifices, an acceptable distribution may result within the practical limits of low pressure drop. Based on a maximum deviation of approximately 4 percent, an orifice-to-manifold area ratio

$$\frac{A_{o,total}}{A_m} = 0.42 \tag{A3}$$

was determined (see fig. 10 and text) for the TOM and ROM-1 configurations. The quantity $A_{o,total}$ may be calculated by using

$$A_{o,total} = \frac{W}{(C_d)\sqrt{\rho 2(P_s - p_m)_{mean}}} \tag{A4}$$

The value of the orifice pressure drop term, $(P_s - p_m)$ in equation (A4), may be made comparable to or less than that used with inlet manifolds. Discharge coefficient values C_d are obtained from figure 14(a) for a selected orifice diameter; the fluid density ρ is based on boiler outlet conditions. The derived value of $A_{o,total}$ is used in equation (A3) to obtain manifold cross-sectional area. Although manifold cross-sectional shape is somewhat arbitrary, the dimension perpendicular to the orifice surface should be greater than orifice diameter; otherwise, discharge coefficient values may be affected.

For an ideal flow distribution each orifice area is adjusted to compensate for static pressure variation along the manifold. The effects of both flow acceleration and mixing losses (refs. 9 and 11) on static pressure must be considered. The individually determined orifice pressure drops may then be used in equation (A4) to size each orifice for an equally apportioned flow rate W.

REFERENCES

1. Hess, H. L.; Kunz, H. R.; and Wyde, S. S.: Analytical Study of Liquid Metal Condensers. Vol. 1: Design Study. Rep. PWA-2320, vol. 1, Pratt & Whitney Aircraft (NASA CR-54224), July 15, 1964.

2. Keller, J. D.: The Manifold Problem. J. Appl. Mech., vol. 16, no. 1, Mar. 1949, pp. 77-85.

3. Markland, E.: The Analysis of Flow From Pipe Manifolds. Engineering, vol. 187, no. 4847, Jan. 30, 1959, pp. 150-151.

4. Dittrich, Ralph T.; and Graves, Charles C.: Discharge Coefficients for Combustor-Liner Air-Entry Holes. I - Circular Holes with Parallel Flow. NACA TN 3663, 1956.

5. Rohde, John E.; Richards, Hadley T.; and Metger, George W.: Discharge Coefficients for Thick Plate Orifices with Approach Flow Perpendicular and Inclined to the Orifice Axis. NASA TN D-5467, 1969.

6. Weske, John R.: Experimental Investigation of Velocity Distributions Downstream of Single Duct Bends. NACA TN-1471, 1948.

7. Higginbotham, James T.; Wood, Charles C.; and Valentine, E. Floyd: A Study of High-Speed Performance Characteristics of 90° Bends in Circular Ducts. NACA TN 3696, 1956.

8. Callaghan, Edmund E.; and Bowden, Dean T.: Investigation of Flow Coefficient of Circular, Square, and Elliptical Orifices at High Pressure Ratios. NACA TN 1947, 1949.

9. Vazsonyi, Andrew: Pressure Loss in Elbows and Duct Branches. Trans. ASME, vol. 66, no. 3, Apr. 1944, pp. 177-183.

10. Zeisser, M. H.: Summary Report of Single-Tube Branch and Multitube Branch Water Flow Tests Conducted by the University of Connecticut. Rep. PWAC-213, Pratt & Whitney Aircraft.

11. Keenan, M. J.: Correlations of Manifold Pressure Loss Data. Rep. APR-1044, Pratt & Whitney Aircraft, Dec. 1962.

TABLE V. - TABULATION

(a) Inlet

Run	Fluid density, ρ, kg/m^3	Reference velocity at station a, V_a, m/sec	Reference velocity head at station a, $(P_a - p_a)$, N/m^2	Total pressure loss between station a and orifice number, $P_a - P_m$, N/m^2						Manifold local velocity head of approach flow at orifice number, $P_m - p_m$, N/m^2					
				Station						Station					
				1	2	3	4	5	6	1	2	3	4	5	6
Tangential inlet manifold (TIM); orifice A;															
439	989	0.384	72.92	17.5	28.2	16.1	17.4	21.8	21.8	19.2	8.47	2.10	74.8	51.9	33.4
440	989	.671	222.6	20.9	34.0	34.5	2.2	33.9	33.5	56.9	25.3	6.33	223.6	155	99.8
441	987	.980	474.1	28.0	76.0	61.0	-11.9	59.0	47.0	119.9	53.6	13.5	473.3	329	212
442	987	1.255	777.2	36.0	128.0	101.0	-6.0	103	110	197.8	87.7	21.8	775.8	438	346
Tangential inlet manifold (TIM); orifice B;															
435	994	0.453	102.0	4.39	17.8	8.06	1.02	13.4	20.5	25.2	11.8	3.0	103	71.7	46.1
436	992	.830	341.9	19.2	49.1	41.3	-14.7	33.6	27.1	87.4	39.0	9.8	343	239	154
437	991	1.089	588.0	40.0	85.7	61.7	-11.7	74.6	74.0	150	67.3	16.7	590	411	264
438	990	1.501	1115	70.2	135	138	-42.4	149	133	285	128	31.8	1118	780	501
Tangential inlet manifold (TIM); orifice C;															
331	992	0.512	130.0	23.4	42.3	35.2	0.81	20.6	15.5	34.2	15.3	3.9	131	92.5	60.6
332	991	.753	281.0	26.2	85.3	54.7	2.82	49.3	62.4	74.0	33.2	8.3	282.2	198.7	130.1
333	990	1.088	586.2	35.2	83.2	59.8	-11.1	89.0	76.0	153.0	68.5	17.4	587.1	413.2	270.4
334	989	1.506	1122	51.6	121	125	-38.1	146	104	292.3	131.3	33.6	1122	790	517
335	988	1.868	1724	58.6	123	89.7	-86.2	204	163	452.6	203.1	50.6	1725	1213	792.1
336	987	2.338	2698	89.0	108	108	-122	308	225	708.2	318.7	79.3	2694	1894	1238
Tangential inlet manifold (TIM) (beginning of test);															
128	995	0.649	210	9.0	22.0	5.0	-1	43.0	39.0	56.2	24.9	6.3	211	149	98.2
129	993	.911	412	31	56	57	-22	67	58	110	49.4	12.4	416	291	192
130	991	1.253	778	102	161	139	14	160	130	205	92	22.8	781	545	358
131	991	1.579	1235	59	111	94	-77	151	105	325	146	36.7	1239	866	569
132	988	1.853	1696	93	210	126	-79	225	158	445	201	49.7	1685	1182	778
133	986	2.137	2251	119	210	140	-113	294	199	594	268	66.4	2256	1577	1039
134	984	2.499	3073	146	138	122	-124	437	318	809	365	90.9	3057	2145	1414
135	983	2.859	4016	228	140	148	-158	571	421	1055	477	118.0	3993	2801	1842
Tangential inlet manifold (TIM) (near end of test);															
403	994	0.621	191.7	14.0	42.2	40.8	1.2	40.6	50.0	51.0	22.8	5.8	193	135	88.9
404	993	1.115	617.2	18.8	54.3	53.3	-30.9	59.7	44.7	164	73	18.5	621	437	286
405	992	1.538	1173	29.3	90	64.6	-81	118	74	311	139	35.3	1179	832	543
406	991	1.876	1743	47.1	101	109	-108	186	111	464	207	51.8	1748	1232	808
Tangential inlet manifold (TIM); orifice E;															
206	994	0.579	166	30.9	37.1	34.0	38.2	50.1	52.8	45.1	20.4	5.0	167	118	78.7
207	992	.850	358	26.3	79.6	56.8	4.2	71.4	46.1	96.8	43.5	10.8	359	255	170
208	991	1.207	722	38.2	90.0	62.8	-9.9	107.2	76.3	195	87.4	22.1	724	514	342
209	988	1.564	1209	50.8	138	99.2	-34.6	167	102	326	146	37.2	1206	856	570
210	987	1.935	1848	81	153	98.8	-82	231	132	500	225	56.9	1846	1311	874
211	985	2.259	2514	99	100	33.3	-100	315	205	677	306	77.1	2503	1775	1181
212	983	2.743	3700	5	-133	-146	-220	386	201	998	452	114	3682	2614	1745
Tangential inlet manifold (TIM); orifice F;															
325	996	0.576	165	26.7	52.4	50.8	37.4	64.7	48.2	48.0	22.3	5.4	166	121	82.0
326	995	.993	433	18.0	29.6	36.4	3.2	66.8	39.3	125	58.2	14.4	436	317	215
327	994	1.286	822	22.2	38.6	29.6	-29.6	86.2	38.6	239	111	27.7	827	600	407
328	993	1.728	1482	22.2	66.7	48.9	-75.7	148	68.3	429	198	50.1	1488	1079	732
329	992	2.234	2476	54.5	15.8	-49	-141	248	124	720	334	84.4	2488	1803	1225
330	991	2.630	3428	-11	-87	-56	-195	342	143	996	462	117	3436	2492	1693

OF EXPERIMENTAL DATA

manifolds

Orifice jet velocity head, $P_{m(average)} - p_s$ N/m^2	Theoretical mass flow rate per orifice, W_t, kg/sec	Measured mass flow rate at orifice number, W_j, kg/sec						Reynolds number at reference station a, Re, dimensionless	Run
		Station							
		1	2	3	4	5	6		
diameter, 1.59 cm; area, 1.982 cm^2									
5 260	0.639	0.3846	0.3824	0.3797	0.3778	0.3742	0.3661	42×10^3	439
15 810	1.108	.6951	.6582	.6586	.6523	.6428	.6400	75	440
33 900	1.623	.9598	.9566	.9603	.9480	.9349	.9371	115	441
55 640	2.079	1.231	1.229	1.223	1.218	1.202	1.191	149	442
diameter, 1.91 cm; area, 2.854 cm^2									
3 550	0.756	0.4418	0.448	0.452	0.435	0.440	0.435	39×10^3	435
12 100	1.395	.8124	.816	.820	.805	.804	.796	79	436
20 830	1.830	1.061	1.078	1.071	1.054	1.051	1.046	107	437
39 180	2.510	1.462	1.482	1.477	1.447	1.448	1.442	158	438
diameter, 2.28 cm; area, 4.100 cm^2									
2 260	0.866	0.504	0.512	0.514	0.476	0.480	0.509	49×10^3	331
4 910	1.277	.743	.753	.756	.708	.704	.735	76	332
10 190	1.839	1.071	1.075	1.093	1.022	1.017	1.067	114	333
19 780	2.565	1.476	1.484	1.517	1.413	1.406	1.477	163	334
30 450	3.181	1.839	1.869	1.863	1.755	1.751	1.799	210	335
48 300	4.006	2.294	2.343	2.332	2.193	2.183	2.246	274	336
orifice D; diameter, 2.54 cm; area, 5.077 cm^2									
2 400	1.106	0.656	0.650	0.657	0.608	0.601	0.632	53×10^3	128
4 650	1.539	.905	.919	.922	.870	.842	.882	82	129
8 879	2.127	1.239	1.260	1.252	1.203	1.158	1.207	125	130
14 280	2.697	1.560	1.575	1.586	1.513	1.457	1.529	162	131
19 550	3.156	1.816	1.864	1.847	1.746	1.696	1.780	213	132
25 990	3.639	2.093	2.157	2.134	2.018	1.957	2.058	264	133
35 040	4.226	2.443	2.510	2.497	2.356	2.277	2.399	325	134
46 210	4.853	2.786	2.869	2.850	2.683	2.624	2.735	390	135
orifice D; diameter, 2.54 cm; area, 5.077 cm^2									
2.290	1.085	0.619	0.624	0.628	0.583	0.584	0.599	54×10^3	403
7 450	1.955	1.116	1.110	1.127	1.049	1.046	1.076	104	404
14 150	2.693	1.538	1.527	1.556	1.446	1.439	1.484	149	405
21 040	3.286	1.874	1.881	1.885	1.757	1.748	1.805	193	406
diameter, 2.86 cm; area, 6.415 cm^2									
1 293	1.026	0.576	0.596	0.587	0.533	0.527	0.563	51×10^3	206
2 773	1.502	.849	.866	.862	.782	.770	.832	82	207
5 660	2.146	1.206	1.216	1.232	1.110	1.095	1.186	124	208
9 528	2.784	1.556	1.572	1.597	1.431	1.410	1.529	176	209
14 590	3.445	1.927	1.953	1.976	1.769	1.739	1.887	227	210
19 940	4.027	2.233	2.284	2.299	2.070	2.031	2.185	284	211
28 570	4.820	2.704	2.768	2.800	2.503	2.449	2.667	363	212
diameter, 3.18 cm; area, 7.917 cm^2									
912	1.063	0.576	0.628	0.610	0.497	0.509	0.557	45×10^3	325
2 371	1.714	.933	1.003	.995	.809	.820	.909	77	326
4 575	2.379	1.293	1.376	1.377	1.116	1.133	1.236	111	327
8 223	3.193	1.734	1.834	1.853	1.499	1.516	1.665	160	328
13 840	4.140	2.240	2.379	2.406	1.941	1.956	2.139	215	329
19 350	4.900	2.636	2.794	2.836	2.278	2.298	2.509	264	330

TABLE V. - Continued. TABULATION

(a) Continued. Inlet

Run	Fluid density, ρ, kg/m^3	Reference velocity at station a, V_a, m/sec	Reference velocity head at station a, $(P_a - p_a)$, N/m^2	Total pressure loss between station a and orifice number, $P_a - P_m$, N/m^2						Manifold local velocity head of approach flow at orifice number, $P_m - p_m$, N/m^2					
				Station						Station					
				1	2	3	4	5	6	1	2	3	4	5	6
Radial inlet manifold (RIM-1); orifice A;															
443	990	0.357	63.1	34.9	56.1	54.8	34.9	37.6	37.9	28.2	62.5	63.8	28.2	7.0	6.7
444	988	.695	239	60.7	132	149	78.7	103	122	106	238	239	106	25.9	26
445	987	.993	487	128	265	315	143	196	197	214	483	488	218	52.9	52.2
446	986	1.269	794	229	473	558	260	343	363	348	788	796	354	86.0	85.1
Radial inlet manifold (RIM-1); orifice B;															
431	987	0.474	111	61.8	112	111	79	99	99	49.0	110	111	50.0	12.5	12.2
432	985	.817	329	111	244	222	126	164	165	146	326	330	148	36.9	35.8
433	985	1.095	590	185	433	371	180	250	270	260	585	592	265	66.1	63.9
434	985	1.555	1191	305	778	762	348	455	477	524	1179	1195	536	134	130
Radial inlet manifold (RIM-1); orifice C;															
166	994	0.802	320	103	206	232	100	155	173	144	318	329	147	36.8	36.8
167	993	1.00	496	145	281	422	178	238	238	224	495	502	228	56.9	57.0
168	990	1.256	781	209	397	718	282	326	346	355	777	788	356	90.1	89.1
169	988	1.530	1156	306	626	1101	376	474	496	524	1146	1168	528	134	131
170	986	1.868	1719	347	910	1640	590	686	642	793	1729	1700	772	195	201
171	984	2.444	2938	590	1578	2810	922	1110	972	1353	2952	2902	1317	332	343
172	983	1.384	941	220	467	907	322	379	375	431	942	927	422	106	109
Radial inlet manifold (RIM-1) (beginning of test);															
109	990	0.716	254	134	192	240	154	208	189	120	261	249	118	27.9	28.8
110	988	.914	413	165	299	368	202	258	257	194	422	407	193	46.8	47.8
111	987	1.134	634	229	462	532	263	342	341	296	642	626	298	74.4	74.6
112	996	1.402	980	224	585	647	263	360	357	466	992	984	463	113	116
113	995	1.655	1363	314	871	918	354	516	495	651	1379	1368	647	159	162
114	994	1.938	1865	529	1228	1481	661	818	778	884	1886	1869	879	215	219
115	992	2.301	2624	643	1683	1925	812	1056	995	1239	2642	2619	1233	301	308
116	989	2.786	3838	769	2384	3148	1281	1553	1318	1802	3879	3803	1797	439	457
Radial inlet manifold (RIM-1) (near end of test);															
464	989	0.718	255	81.1	168	222	62.0	134	134	120	254	257	121	30.0	29.5
465	988	1.086	583	147	354	464	162	241	242	273	584	585	276	68.4	67.2
466	987	1.446	1032	240	678	778	309	381	401	485	1026	1037	490	121	120
467	986	1.843	1674	382	1105	1327	529	639	621	785	1671	1670	786	195	195
Radial inlet manifold (RIM-1); orifice E;															
215	987	0.655	212	87	183	203	107	131	130	106	214	212	105	26	27
216	986	.984	477	164	367	468	204	236	251	242	482	474	239	58	61
217	985	1.414	984	271	720	904	353	444	439	496	990	972	488	120	125
218	982	1.789	1572	402	1082	1503	575	687	678	790	1571	1556	784	191	200
219	983	2.146	2265	600	1601	2182	873	984	887	1140	2265	2239	1126	275	298
220	983	2.508	3090	302	1703	2728	801	928	816	1557	3096	3051	1539	376	396
Radial inlet manifold (RIM-1); orifice F;															
311	989	1.100	598	171	460	525	206	281	282	320	604	595	322	81	80
312	988	1.494	1102	290	843	944	369	477	457	595	1114	1087	590	149	151
313	987	1.862	1711	449	1336	1475	564	690	693	918	1713	1704	914	233	230
314	987	2.143	2266	579	1714	2084	840	968	918	1216	2263	2263	1232	309	304
315	986	2.347	2715	704	2117	2518	950	1119	1097	1468	2736	2686	1462	369	372
316	984	1.497	1103	309	861	1023	427	515	513	595	1115	1083	588	149	151

manifolds

Orifice jet velocity head, $P_{m(average)} - P_s$ N/m^2	Theoretical mass flow rate per orifice, W_t, kg/sec	Measured mass flow rate at orifice number, W_j, kg/sec						Reynolds number at reference station a, Re, dimensionless	Run
		Station							
		1	2	3	4	5	6		
diameter, 1.59 cm; area, 1.982 cm^2									
4 370	0.583	0.349	0.345	0.351	0.348	0.347	0.340	38×10^3	443
16 530	1.133	.677	.674	.677	.682	.666	.668	84	444
33 910	1.624	.968	.964	.963	.979	.952	.946	118	445
55 580	2.078	1.236	1.231	1.232	1.248	1.214	1.208	157	446
diameter, 1.91 cm; area, 2.854 cm^2									
3 843	0.786	0.460	0.458	0.455	0.463	0.463	0.457	56×10^3	431
11 450	1.357	.796	.786	.786	.796	.796	.783	102	432
20 450	1.813	1.065	1.055	1.053	1.068	1.064	1.047	140	433
41 230	2.576	1.511	1.498	1.495	1.516	1.515	1.487	199	434
diameter, 2.28 cm; area, 4.100 cm^2									
5 654	1.371	0.779	0.763	0.770	0.787	0.794	0.794	70×10^3	166
8 709	1.701	.974	.951	.958	.988	.988	.988	95	167
13 850	2.145	1.231	1.183	1.204	1.229	1.243	1.236	131	168
20 650	2.619	1.498	1.435	1.465	1.495	1.515	1.500	176	169
31 510	3.325	1.833	1.757	1.760	1.811	1.827	1.855	233	170
52 990	4.196	2.390	2.298	2.302	2.367	2.385	2.426	323	171
16 950	2.373	1.350	1.300	1.298	1.342	1.347	1.368	188	172
orifice D; diameter, 2.54 cm; area, 5.077 cm^2									
2 983	1.234	0.734	0.678	0.645	0.729	0.691	0.703	76×10^3	109
4 850	1.571	.917	.866	.824	.921	.895	.905	103	110
7 503	1.955	1.121	1.066	1.015	1.130	1.130	1.131	136	111
11 640	2.436	1.416	1.296	1.289	1.425	1.393	1.412	104	112
16 180	2.871	1.677	1.521	1.515	1.679	1.651	1.655	135	113
21 320	3.296	1.957	1.792	1.778	1.962	1.920	1.937	180	114
30 140	3.919	2.310	2.122	2.104	2.326	2.271	2.298	232	115
44 030	4.736	2.759	2.597	2.525	2.808	2.742	2.799	308	116
orifice D; diameter, 2.54 cm; area, 5.077 cm^2									
3 110	1.264	0.722	0.656	0.659	0.721	0.717	0.711	78×10^3	464
7 105	1.909	1.092	.990	.993	1.091	1.082	1.073	125	465
12 720	2.555	1.450	1.313	1.319	1.455	1.442	1.432	172	466
20 740	3.261	1.842	1.684	1.681	1.842	1.829	1.827	228	467
diameter, 2.86 cm; area, 6.415 cm^2									
1 795	1.208	0.672	0.563	0.556	0.679	0.644	0.679	77×10^3	215
3 990	1.802	1.011	.840	.828	1.022	1.000	1.024	120	216
8 273	2.594	1.450	1.204	1.189	1.462	1.432	1.466	181	217
13 320	3.291	1.829	1.509	1.502	1.852	1.811	1.852	244	218
19 214	3.953	2.194	1.810	1.801	2.222	2.172	2.227	284	219
25 950	4.595	2.564	2.118	2.096	2.596	2.540	2.604	343	220
diameter, 3.18 cm; area, 7.917 cm^2									
3 641	2.123	1.172	0.877	0.846	1.171	1.178	1.169	122×10^3	311
6 617	2.865	1.584	1.177	1.137	1.583	1.597	1.610	181	312
10 450	3.597	1.980	1.452	1.420	1.987	1.988	1.986	220	313
13 860	4.144	2.282	1.662	1.633	2.292	2.303	2.284	255	314
16 670	4.544	2.490	1.832	1.780	2.492	2.514	2.527	289	315
6 817	2.908	1.584	1.177	1.134	1.578	1.597	1.611	194	316

TABLE V. - Continued. TABULATION

(a) Concluded. Inlet

Run	Fluid density, ρ, kg/m^3	Reference velocity at station a, V_a, m/sec	Reference velocity head at station a, $(P_a - p_a)$, N/m^2	Total pressure loss between station a and orifice number, $P_a - P_m$, N/m^2						Manifold local velocity head of approach flow at orifice number, $P_m - p_m$, N/m^2					
				Station						Station					
				1	2	3	4	5	6	1	2	3	4	5	6
Radial inlet manifold (RIM-2); orifice A;															
446	994	0.351	61.2	27.6	19.1	------	19.7	28.0	41.4	15.5	42.5	--------	41.9	15.1	1.7
447	993	.673	225	95.8	70.4	------	108	116	146	56.7	156	--------	155	55.3	6.2
448	992	.964	461	164	109	------	175	167	249	116	319	--------	290	113	12.8
Radial inlet manifold (RIM-2); orifice B;															
427	992	0.500	124	57	39	------	59	58	85	31	86	--------	84	30	3
428	991	.831	342	131	92	------	129	131	224	85	235	--------	235	84	9
429	990	1.087	585	223	152	------	228	243	353	145	401	--------	399	143	16
430	988	1.507	1122	373	270	------	516	488	621	278	769	--------	764	274	30
Radial inlet manifold (RIM-2); orifice C;															
175	993	0.792	311	142	118	------	137	160	212	79	214	--------	213	80	9
176	991	1.012	508	216	184	------	201	233	386	128	346	--------	346	130	14
177	989	1.250	773	287	229	------	331	325	443	196	530	--------	522	194	21
178	988	1.487	1092	401	322	------	476	477	592	275	744	--------	738	274	30
179	985	2.371	2769	894	704	------	1072	1083	1443	698	1888	--------	1870	695	76
Radial inlet manifold (RIM-2) (beginning of test);															
119	987	1.012	505	219	190	------	187	220	292	123	333	--------	336	122	14
120	985	1.295	826	371	372	------	278	355	515	202	545	--------	548	200	22
121	983	1.606	1268	487	471	------	370	455	636	310	833	--------	843	306	34
122	982	1.838	1658	659	680	------	450	590	884	402	1087	--------	1100	400	45
123	987	2.134	2247	883	989	------	603	779	1137	550	1481	--------	1500	545	61
124	985	2.420	2887	1118	1158	------	803	1068	1416	701	1892	--------	1921	697	78
125	984	2.783	3811	1492	1586	------	1023	1370	1880	925	2496	--------	2534	920	103
Radial inlet manifold (RIM-2) (near end of test);															
454	994	0.706	248	99	64	------	83	96	132	59	167	--------	167	62	7
455	994	1.127	631	220	178	------	230	240	324	158	422	--------	425	156	17
456	992	1.459	1056	357	286	------	392	415	538	265	706	--------	711	262	29
457	991	1.900	1788	582	476	------	661	680	851	446	1200	--------	1200	440	48
Radial inlet manifold (RIM-2); orifice E;															
223	982	0.768	290	165	143	------	163	167	228	71	186	--------	184	69	8
224	983	1.195	701	293	163	------	332	334	409	173	451	--------	448	169	20
225	994	1.189	702	291	243	------	334	334	429	176	464	--------	447	170	20
226	993	1.603	1275	483	426	------	545	532	713	321	840	--------	814	309	36
227	991	2.048	2078	727	365	------	856	867	1093	518	1368	--------	1332	507	59
228	989	2.447	2962	977	-229	------	1332	1270	1592	736	1942	--------	1897	720	84
Radial inlet manifold (RIM-2); orifice F;															
318	995	0.817	332	141	120	------	170	161	214	82	214	--------	201	81	9
319	994	1.158	666	247	227	------	304	286	376	166	426	--------	405	164	19
320	993	1.628	1315	463	402	------	585	542	698	327	832	--------	797	322	37
321	992	2.048	2079	728	658	------	928	846	1076	518	1328	--------	1261	511	59
322	991	2.481	3050	1008	937	------	1428	1286	1661	757	1937	--------	1853	756	86
323	991	2.682	3565	1233	1169	------	1651	1530	1925	884	2261	--------	2167	883	100
324	990	1.271	800	294	275	------	394	387	487	198	513	--------	486	198	23

manifolds

Orifice jet velocity head, N/m^2		Theoretical mass flow rate per orifice, W_t, kg/sec		Measured mass flow rate at orifice number, W_j, kg/sec						Reynolds numbers at reference station a, Re, dimensionless	Run
$P_{m(average)} - p_s$ (All except station 3)	$P_a - p_s$ (Station 3 only)	All except station 3	Station 3	Station							
				1	2	3	4	5	6		
diameter, 1.59 cm; area, 1.982 cm^2											
4 201	4 224	0.571	0.573	0.344	0.339	0.352	0.338	0.338	0.343	31×10^3	446
15 870	15 950	1.111	1.113	.659	.649	.672	.656	.647	.655	62	447
32 180	32 360	1.581	1.586	.943	.928	.962	.940	.923	.936	95	448
diameter, 1.91 cm; area, 2.854 cm^2											
4 258	4 380	0.828	0.839	0.488	0.485	0.508	0.478	0.483	0.477	48×10^3	427
12 000	12 340	1.389	1.409	.809	.801	.839	.804	.807	.789	85	428
20 400	20 990	1.811	1.838	1.056	1.047	1.101	1.051	1.046	1.039	116	429
38 610	39 740	2.492	2.528	1.461	1.448	1.521	1.450	1.446	1.444	173	430
diameter, 2.28 cm; area, 4.100 cm^2											
5 450	5 542	1.346	1.357	0.776	0.754	0.809	0.740	0.782	0.773	73×10^3	175
8 894	9 086	1.719	1.737	.988	.954	1.032	.944	.996	.990	102	176
13 692	13 990	2.133	2.156	1.225	1.182	1.277	1.168	1.218	1.212	138	177
19 450	19 860	2.543	2.568	1.457	1.399	1.519	1.390	1.459	1.431	172	178
48 270	49 320	4.005	4.048	2.315	2.231	2.408	2.210	2.308	2.288	298	179
orifice D; diameter, 2.54 cm; area, 5.077 cm^2											
5 634	5 826	1.694	1.723	0.971	0.935	1.085	0.951	0.967	0.965	121×10^3	119
9 309	9 623	2.178	2.214	1.241	1.199	1.394	1.214	1.232	1.236	166	120
14 270	14 750	2.697	2.743	1.539	1.474	1.721	1.510	1.526	1.531	216	121
19 270	19 900	3.133	3.196	1.753	1.689	1.968	1.724	1.742	1.748	257	122
25 610	26 470	3.612	3.673	2.047	1.969	2.296	2.013	2.035	2.046	254	123
32 570	33 670	4.074	4.142	2.315	2.227	2.603	2.282	2.303	2.305	304	124
43 730	45 180	4.720	4.797	2.656	2.560	2.993	2.620	2.645	2.651	361	125
orifice D; diameter, 2.54 cm; area, 5.077 cm^2											
2 869	2 963	1.214	1.235	0.692	0.657	0.754	0.664	0.686	0.682	61×10^3	454
7 341	7 581	1.941	1.972	1.102	1.046	1.205	1.061	1.095	1.087	102	455
12 330	12 730	2.514	2.557	1.427	1.350	1.558	1.371	1.417	1.407	141	456
20 980	21 660	3.282	3.334	1.858	1.768	2.020	1.785	1.841	1.815	195	457
diameter, 2.86 cm; area, 6.415 cm^2											
2 170	2 281	1.329	1.362	0.735	0.682	0.874	0.687	0.721	0.735	107×10^3	223
5 286	5 552	2.073	2.125	1.144	1.058	1.357	1.068	1.124	1.160	163	224
5 250	5 517	2.066	2.119	1.157	1.080	1.365	1.061	1.126	1.163	105	225
9 605	10 090	2.795	2.886	1.563	1.499	1.849	1.436	1.518	1.563	152	226
15 700	16 490	3.573	3.659	1.977	1.862	2.330	1.831	1.943	2.008	210	227
22 420	23 540	4.270	4.375	2.355	2.218	2.778	2.188	2.317	2.393	266	228
diameter, 3.18 cm; area, 7.917 cm^2											
1 654	1 780	1.433	1.485	0.790	0.727	1.010	0.680	0.781	0.795	68×10^3	318
3 327	3 580	2.031	2.077	1.123	1.013	1.442	.961	1.109	1.131	100	319
6 625	7 125	2.865	2.971	1.570	1.409	2.036	1.346	1.554	1.593	154	320
10 630	11 420	3.629	3.763	1.977	1.792	2.544	1.688	1.958	2.005	202	321
15 630	16 790	4.400	4.562	2.387	2.161	3.087	2.037	2.385	2.430	250	322
18 430	19 780	4.780	4.953	2.580	2.334	3.346	2.205	2.578	2.623	270	223
4 062	4 366	2.242	2.327	1.221	1.122	1.565	1.045	1.218	1.243	133	324

TABLE V. - Continued. TABULATION

(b) Outlet

Run	Fluid density, ρ, kg/m^3	Velocity head of jet orifice number, $P_s - p_m$, N/m^2						Velocity head of manifold flow leaving orifice number, $P_m - p_m$, N/m^2						Total pressure loss between orifice number and station a, $P_m - P_a$, N/m^2					
		Station						Station						Station					
		1	2	3	4	5	6	1	2	3	4	5	6	1	2	3	4	5	6
Tangential outlet manifold (TOM); orifice																			
69	994	4 176	4 176	4 121	4 121	4 102	3 973	133	92	58	32	14	4						
70	993	6 534	6 497	6 423	6 403	6 405	6 220	209	145	92	51	23	6						
71	991	8 981	9 053	8 981	9 000	8 778	8 537	297	205	130	73	32	8						
72	990	19 270	19 360	18 950	18 970	18 950	18 420	604	418	266	149	65	17	Not available					
73	989	37 820	37 970	37 300	37 210	36 080	36 010	1182	818	521	290	128	33						
74	987	61 640	61 880	60 860	60 530	60 550	58 780	1939	1343	855	477	210	53						
75	986	95 490	95 680	93 830	93 590	94 000	91 070	2967	2055	1307	729	321	82						
76	985	99 240	99 620	97 900	97 650	97 740	94 760	3128	2138	1360	759	334	85						
Tangential outlet manifold (TOM); orifice																			
254	994	1 593	1 591	1 480	1 480	1 480	1 464	105	72	45	25	11	3	55	114	106	86	72	82
255	992	4 434	4 194	4 120	4 100	4 120	4 064	298	206	129	72	32	8	146	294	291	253	194	226
256	991	8 905	8 353	8 258	8 239	8 276	8 128	588	406	256	142	63	16	295	668	610	515	399	500
257	990	15 240	14 280	14 110	14 075	14 060	13 870	995	689	434	241	106	27	489	1143	1060	900	783	889
258	989	23 230	21 620	21 470	21 420	21 290	21 010	1523	1052	664	369	163	41	636	1774	1533	1294	1217	1373
259	989	40 660	37 840	37 530	37 460	37 270	36 620	2626	1816	1147	636	281	71	1177	3177	2823	2386	2216	2653
260	988	5 010	4 718	4 663	4 663	4 607	4 552	337	231	145	81	35	9	168	358	327	263	273	302
Tangential outlet manifold (TOM); orifice																			
78	993	2 754	2 569	2 495	2 477	2 532	2 440	282	190	118	65	29	7	144	237	239	204	113	183
79	992	4 860	4 527	4 379	4 379	4 416	4 287	506	342	212	118	52	13	306	475	493	399	296	486
80	991	6 823	6 379	6 120	6 046	6 120	6 028	682	457	282	154	66	19	460	679	763	709	547	591
81	989	8 694	8 317	8 002	7 984	8 002	7 892	910	614	383	212	94	24	540	891	975	822	686	726
82	988	12 320	11 520	11 140	10 990	11 060	10 910	1247	840	524	291	129	32	738	1128	1200	1115	879	930
83	985	17 310	16 180	15 680	15 530	15 620	15 500	1709	1155	722	400	177	45	998	1572	1638	1464	1149	1146
84	984	22 810	21 330	20 630	20 330	20 640	20 140	2180	1515	945	523	232	59	1313	2127	2260	2134	1528	1855
85	984	28 290	26 570	25 610	25 300	25 480	25 130	2847	1922	1199	664	294	74	1771	2566	2804	2546	2028	2160
86	983	37 030	34 590	33 480	32 890	33 570	32 590	3700	2496	1557	863	383	97	2319	3556	3726	3624	2460	3154
Tangential outlet manifold (TOM); orifice																			
246	987	941	830	793	793	793	756	135	89	55	30	13	3	16	81	84	59	42	69
247	987	1 936	1 714	1 603	1 585	1 585	1 492	296	197	119	65	29	7	106	229	262	226	190	261
248	986	4 181	3 663	3 460	3 386	3 423	3 238	643	422	256	140	62	15	236	533	570	523	413	551
249	988	6 389	5 649	5 298	5 169	5 224	4 865	985	647	393	215	95	24	378	780	877	828	652	840
250	987	9 321	8 212	7 731	7 491	7 583	7 269	1407	924	561	307	135	33	522	1148	1266	1252	988	1200
251	987	15 630	13 840	12 910	12 560	12 760	12 250	2363	1553	940	513	226	56	1029	2013	2324	2248	1758	2106
252	987	24 700	21 700	20 350	19 870	20 090	19 130	3785	2487	1505	822	361	90	1584	3281	3649	3447	2764	3454
Tangential outlet manifold (TOM); orifice																			
286	992	869	740	629	592	592	573	189	122	73	39	17	4	54	116	178	181	159	165
287	991	1 683	1 424	1 239	1 184	1 184	1 128	357	230	138	74	32	8	128	260	353	344	302	334
288	990	3 385	2 867	2 516	2 368	2 368	2 257	732	473	282	152	66	16	218	477	637	655	569	630
289	989	6 082	5 139	4 510	4 252	4 252	4 030	1283	828	495	266	116	29	381	869	1165	1194	1044	1179
290	988	8 688	7 388	6 488	6 062	6 081	5 767	1826	1179	703	377	164	41	562	1265	1639	1739	1507	1698
291	988	18 210	15 360	13 580	12 750	12 850	12 180	3761	2430	1449	774	337	84	1177	2693	3488	3645	3115	3528
292	988	12 344	10 370	9 164	8 609	8 664	8 239	2564	1666	993	532	231	58	793	1873	2403	2496	2140	2392

manifolds

Reference velocity head at station a, $P_a - p_a$, N/m^2	Theoretical mass flow rate at orifice number, W_t, kg/sec						Reference velocity at station a, V_a, m/sec	Measured mass flow rate at orifice number, W_j, kg/sec						Reynolds number at reference station a, Re, dimensionless	Run
	Station							Station							
	1	2	3	4	5	6		1	2	3	4	5	6		
B; diameter, 1.91 cm; area, 2.854 cm^2															
132	0.820	0.820	0.814	0.814	0.813	0.800	0.515	0.508	0.516	0.507	0.497	0.494	0.496	45.6×10^3	69
209	1.025	1.022	1.016	1.015	1.015	1.000	.649	.640	.641	.637	.627	.626	.617	61.3	70
297	1.202	1.206	1.202	1.204	1.189	1.172	.774	.760	.762	.755	.749	.735	.749	79.5	71
602	1.761	1.766	1.746	1.746	1.746	1.723	1.103	1.084	1.083	1.077	1.074	1.049	1.069	119	72
1180	2.468	2.473	2.451	2.450	2.443	2.410	1.545	1.515	1.512	1.515	1.502	1.467	1.493	172	73
1940	3.152	3.158	3.130	3.125	3.125	3.078	1.984	1.937	1.939	1.939	1.923	1.882	1.912	232	74
2980	3.922	3.925	3.887	3.883	3.893	3.830	2.457	2.395	2.402	2.397	2.379	2.327	2.365	298	75
3090	4.000	4.008	3.972	3.966	3.970	3.909	2.505	2.440	2.449	2.445	2.427	2.377	2.409	315	76
C; diameter, 2.28 cm; area, 4.100 cm^2															
104	0.728	0.728	0.701	0.701	0.701	0.697	0.457	0.453	0.470	0.448	0.439	0.438	0.435	40.5×10^3	254
297	1.213	1.180	1.171	1.167	1.171	1.163	.774	.764	.783	.755	.744	.735	.740	74.9	255
583	1.720	1.665	1.656	1.651	1.657	1.643	1.085	1.074	1.089	1.063	1.048	1.031	1.046	109	256
994	2.251	2.177	2.168	2.162	2.160	2.148	1.417	1.389	1.417	1.388	1.367	1.343	1.357	149	257
1520	2.780	2.681	2.672	2.670	2.660	2.641	1.753	1.725	1.745	1.719	1.691	1.664	1.676	190	258
2625	3.680	3.550	3.532	3.528	3.520	3.489	2.304	2.256	2.293	2.266	2.214	2.179	2.221	255	259
332	1.289	1.249	1.245	1.245	1.238	1.230	.820	.806	.821	.799	.798	.777	.783	94.1	260
D; diameter, 2.54 cm; area, 5.077 cm^2															
282	1.184	1.143	1.128	1.122	1.135	1.114	0.753	0.792	0.762	0.730	0.700	0.704	0.712	68.4×10^3	78
505	1.573	1.517	1.492	1.492	1.500	1.476	1.009	1.051	1.025	.972	.947	.943	.953	98.6	79
707	1.864	1.803	1.764	1.753	1.764	1.750	1.195	1.243	1.201	1.150	1.118	1.112	1.125	123.0	80
909	2.104	2.058	2.019	2.016	2.019	2.003	1.356	1.415	1.361	1.309	1.275	1.263	1.279	150	81
1245	2.507	2.425	1.381	2.366	2.373	2.360	1.588	1.658	1.593	1.529	1.490	1.484	1.493	183	82
1719	2.972	2.873	1.828	2.814	2.822	2.812	1.868	1.932	1.866	1.796	1.751	1.737	1.751	237	83
2253	3.410	3.297	3.242	3.218	3.248	3.208	2.140	2.214	2.145	2.057	2.001	1.984	2.006	278	84
2858	3.798	3.680	3.612	3.590	3.604	3.579	2.411	2.490	2.413	2.316	2.259	2.232	2.259	319	85
3721	4.346	4.200	4.133	4.093	4.138	4.076	2.752	2.842	2.751	2.640	2.570	2.542	2.581	376	86
E; diameter, 2.86 cm; area, 6.415 cm^2															
138	0.875	0.822	0.803	0.803	0.803	0.784	0.528	0.580	0.553	0.502	0.485	0.478	0.471	61.8×10^3	246
299	1.255	1.181	1.141	1.135	1.135	1.102	.778	.860	.816	.738	.716	.705	.697	92.6	247
642	1.844	1.726	1.676	1.660	1.670	1.622	1.140	1.257	1.190	1.087	1.046	1.031	1.027	138	248
987	2.278	2.142	2.073	2.051	2.061	1.991	1.414	1.559	1.470	1.349	1.296	1.275	1.271	162	249
1410	2.753	2.584	2.509	2.469	2.482	2.432	1.689	1.864	1.760	1.611	1.546	1.527	1.516	198	250
2366	3.569	3.355	3.243	3.196	3.223	3.157	2.188	2.411	2.288	2.095	2.000	1.968	1.967	260	251
3794	4.484	4.204	4.103	4.022	4.050	3.947	2.777	3.049	2.895	2.655	2.531	2.488	2.490	330	252
F; diameter, 3.18 cm; area, 7.917 cm^2															
189	1.038	0.958	0.882	0.857	0.857	0.843	0.617	0.706	0.664	0.592	0.561	0.546	0.533	60.7×10^3	286
356	1.445	1.329	1.239	1.212	1.212	1.183	.848	.973	.900	.818	.772	.749	.735	87.0	287
731	2.049	1.885	1.765	1.714	1.714	1.672	1.215	1.390	1.298	1.171	1.097	1.070	1.060	130	288
1282	2.746	2.522	2.367	2.298	2.298	2.235	1.610	1.842	1.713	1.555	1.454	1.410	1.405	176	289
1825	3.282	3.014	2.836	2.744	2.746	2.556	1.922	2.195	2.048	1.857	1.731	1.682	1.675	217	290
3760	4.752	4.367	4.102	3.980	3.992	3.888	2.759	3.149	2.942	2.681	2.480	2.405	2.401	337	291
2567	3.916	3.583	3.370	3.268	3.278	3.195	2.280	2.571	2.440	2.214	2.054	1.993	1.991	264	292

TABLE V. - Continued. TABULATION

(b) Continued. Outlet

Run	Fluid density, ρ, kg/m^3	Velocity head of jet orifice number, $P_s - p_m$, N/m^2						Velocity head of manifold flow leaving orifice number, $P_m - p_m$, N/m^2						Total pressure loss between orifice number and station a, $P_m - P_a$, N/m^2					
		Station						Station						Station					
		1	2	3	4	5	6	1	2	3	4	5	6	1	2	3	4	5	6
Radial outlet manifold (ROM-1); orifice																			
43	995	3 272	3 198	3 198	3 277	3 382	3 364	51	13	12	50	116	118	318	354	353	317	273	293
44	994	5 610	5 554	5 517	5 628	5 794	5 776	82	22	21	84	194	198	546	538	574	526	470	492
45	992	8 198	8 087	7 865	8 106	8 438	8 420	124	31	31	126	287	286	766	784	839	731	689	706
46	989	13 860	13 550	13 640	13 880	14 210	14 200	203	51	49	199	457	464	1128	1290	1196	1105	1031	1056
47	987	24 730	24 210	24 270	24 710	25 320	25 260	369	91	91	372	855	848	2243	2483	2428	2265	2138	2184
48	986	35 290	34 700	34 640	35 460	36 290	36 180	525	129	130	529	1210	1209	3293	3481	3546	3131	2980	3090
49	985	22 340	21 880	21 990	22 420	22 930	22 900	331	82	81	331	759	762	2064	2277	2165	1990	1900	1940
50	984	12 720	12 440	12 500	12 760	13 070	13 070	185	45	45	187	430	430	1202	1340	1284	1167	1096	1096
Radial outlet manifold (ROM-1); orifice																			
262	992	1 285	1 211	1 193	1 303	1 396	1 396	46	11	11	44	104	105	250	290	308	231	198	199
263	991	2 842	2 657	2 657	2 842	3 027	3 027	95	24	24	98	227	224	609	724	724	613	557	554
264	990	6 100	5 712	5 730	6 155	6 470	6 507	208	50	51	209	487	489	1348	1578	1561	1294	1257	1222
265	989	12 350	11 410	11 570	12 350	13 000	13 000	411	98	101	416	970	971	2611	3241	3078	2616	2523	2524
266	988	28 680	26 660	26 700	28 590	30 250	30 250	962	229	234	968	2259	2279	6168	7450	7418	6266	5893	5932
Radial outlet manifold (ROM-1); orifice																			
100	995	1 629	1 500	1 444	1 666	1 795	1 795	83	19	20	81	198	199	498	563	620	459	447	448
101	994	3 312	3 072	2 942	3 349	3 608	3 626	176	42	40	167	405	420	1051	1157	1285	1005	984	981
102	993	5 031	4 624	4 439	5 049	5 438	5 456	265	63	61	259	626	633	1556	1761	1944	1532	1470	1499
103	991	6 697	6 272	5 939	6 734	7.307	7 326	343	81	81	340	825	830	2086	2249	2582	2046	1958	1944
104	988	12 410	11 630	11 020	12 370	13 500	13 460	621	146	147	618	1498	1504	3826	4128	4739	3860	3612	3655
105	986	22 420	20 600	19 880	22 360	24 170	24 230	1110	262	264	1109	2685	2703	6734	7698	8421	6788	6562	6515
106	984	1 915	1 844	1 752	2 010	2 158	2 177	98	23	23	97	236	236	638	674	766	582	573	554
Radial outlet manifold (ROM-1); orifice																			
238	990	660	623	568	697	808	826	59	14	13	56	139	143	362	354	408	322	294	280
239	989	1 502	1 410	1 354	1 576	1 779	1 779	129	30	29	124	309	318	739	732	786	660	642	651
240	988	2 823	2 546	2 546	2 915	3 304	3 341	242	56	53	232	581	600	1426	1517	1514	1324	1284	1266
241	988	4 326	3 993	3 864	4 437	5 347	5 103	375	87	82	357	891	927	2164	2209	2330	2035	1959	1939
242	987	5 991	5 492	5 271	6 065	6 990	7 026	502	115	112	486	1216	1251	2963	3075	3294	2873	2678	2678
243	987	9 008	8 472	7 936	9 230	10 510	10 540	758	173	169	736	1841	1896	4568	4519	5051	4324	4153	4171
244	987	13 060	11 890	11 400	13 370	15 240	15 330	1105	254	247	1074	2692	2767	6644	6958	7450	6299	6049	6032
Radial outlet manifold (ROM-1); orifice																			
279	987	380	343	343	380	491	509	45	9	10	45	117	114	308	310	311	309	270	249
280	986	851	740	722	869	1 091	1 110	104	23	23	102	263	266	599	629	646	579	518	502
281	985	1 593	1 334	1 297	1 593	2 000	2 018	195	43	43	192	498	502	1124	1231	1268	1121	1020	1006
282	984	2 878	2 453	2 416	2 878	3 562	3 655	355	78	77	347	899	914	2015	2163	2199	2007	1875	1797
283	984	4 815	4 075	3 890	4 760	5 961	6 054	597	132	130	584	1518	1547	3472	3747	3930	3514	3247	3183
284	984	8 300	7 227	6 875	8 207	10 280	10 350	988	218	216	972	2529	2567	5850	6152	6502	5926	5413	5377

manifolds

Reference velocity head at station a, $P_a - p_a$, N/m^2	Theoretical mass flow rate at orifice number, W_t, kg/sec						Reference velocity at station a, V_a, m/sec	Measured mass flow rate at orifice number, W_j, kg/sec						Reynolds number at reference station a, Re, dimensionless	Run
	Station							Station							
	1	2	3	4	5	6		1	2	3	4	5	6		
B; diameter, 1.91 cm; area, 2.854 cm^2															
115	0.726	0.717	0.717	0.726	0.738	0.736	0.481	0.468	0.471	0.459	0.469	0.482	0.482	40.0×10^3	43
194	.951	.946	.943	.952	.966	.965	.625	.609	.608	.600	.602	.622	.624	56.6	44
286	1.149	1.140	1.125	1.142	1.165	1.165	.759	.733	.726	.726	.741	.751	.757	73.5	45
459	1.495	1.478	1.484	1.496	1.513	1.514	.963	.930	.934	.914	.931	.951	.956	106	46
852	1.998	1.976	1.979	1.996	2.020	2.019	1.314	1.267	1.249	1.250	1.277	1.302	1.300	154	47
1205	2.398	2.364	2.364	2.390	2.418	2.413	1.570	1.510	1.490	1.492	1.519	1.547	1.556	194	48
765	1.896	1.879	1.882	1.904	1.921	1.922	1.247	1.197	1.184	1.182	1.201	1.225	1.234	159	49
432	1.433	1.415	1.426	1.434	1.451	1.451	.939	.900	.880	.883	.907	.927	.936	124	50
C; diameter, 2.28 cm; area, 4.100 cm^2															
104	0.654	0.635	0.630	0.658	0.681	0.681	0.457	0.447	0.437	0.428	0.443	0.462	0.455	44.2×10^3	262
227	.973	.940	.940	.973	1.002	1.002	.677	.658	.636	.636	.658	.582	.685	68.1	263
489	1.423	1.378	1.379	1.430	1.466	1.471	.994	.962	.927	.931	.962	.996	1.010	105	264
968	2.028	1.948	1.960	2.028	2.079	2.079	1.399	1.356	1.297	1.317	1.355	1.407	1.427	152	265
2269	3.088	2.977	2.981	3.081	3.169	3.167	2.143	2.078	1.983	2.003	2.070	2.150	2.188	242	266
D; diameter, 2.54 cm; area, 5.077 cm^2															
200	0.911	0.874	0.858	0.921	0.957	0.957	0.634	0.622	0.597	0.581	0.600	0.663	0.657	49.4×10^3	100
410	1.298	1.251	1.224	1.306	1.355	1.359	.908	.892	.847	.826	.868	.941	.946	80.5	101
628	1.645	1.535	1.502	1.603	1.662	1.668	1.125	1.092	1.040	1.025	1.084	1.167	1.167	107	102
827	1.849	1.786	1.736	1.851	1.928	1.930	1.292	1.247	1.177	1.179	1.236	1.345	1.350	134	103
1501	2.517	2.439	1.371	2.502	2.623	2.619	1.743	1.680	1.583	1.588	1.668	1.813	1.817	194	104
2702	3.380	3.242	3.182	3.374	3.510	3.517	2.341	2.245	2.118	2.129	2.232	2.428	2.443	284	105
238	.999	.970	.945	1.011	1.048	1.052	.695	.668	.629	.631	.661	.719	.713	91.2	106
E; diameter, 2.86 cm; area, 6.415 cm^2															
141	0.734	0.712	0.680	0.753	0.811	0.820	0.533	0.521	0.482	0.470	0.507	0.565	0.565	56.9×10^3	238
313	1.105	1.071	1.050	1.132	1.203	1.203	.796	.774	.712	.699	.759	.845	.850	93.2	239
590	1.515	1.439	1.439	1.539	1.639	1.649	1.093	1.060	.976	.956	1.040	1.161	1.172	137	240
908	1.875	1.801	1.744	1.898	2.082	2.038	1.356	1.310	1.224	1.187	1.288	1.434	1.453	179	241
1231	2.208	2.111	2.070	2.221	2.385	2.390	1.579	1.532	1.402	1.385	1.502	1.679	1.698	185	242
1873	2.708	2.626	2.539	2.739	2.924	2.928	1.948	1.880	1.724	1.702	1.849	2.067	2.097	228	243
2733	3.258	3.109	3.040	3.300	3.523	3.533	2.353	2.268	2.085	2.058	2.233	2.503	2.535	276	244
F; diameter, 3.18 cm; area, 7.917 cm^2															
116	0.686	0.652	0.652	0.686	0.781	0.794	0.485	0.473	0.400	0.416	0.466	0.534	0.527	57.7×10^3	279
265	1.027	.958	.946	1.037	1.163	1.171	.733	.710	.622	.622	.699	.803	.802	89.5	280
501	1.405	1.285	1.268	1.405	1.575	1.586	1.009	.970	.857	.856	.961	1.105	1.105	128	281
910	1.889	1.744	1.730	1.889	2.102	2.129	1.360	1.309	1.159	1.150	1.290	1.486	1.490	177	282
1541	2.493	2.273	2.197	2.430	2.720	2.740	1.770	1.696	1.504	1.490	1.674	1.937	1.950	234	283
2559	3.210	2.993	2.920	3.187	3.570	3.583	2.281	2.184	1.932	1.924	2.158	2.503	2.518	299	284

TABLE V. - Concluded. TABULATION

(b) Concluded. Outlet

Run	Fluid density, ρ, kg/m^3	Velocity head of jet orifice number, $P_s - p_m$, N/m^2						Velocity head of manifold flow leaving orifice number, $P_m - p_m$, N/m^2						Total pressure loss between orifice number and station a, $P_m - P_a$, N/m^2					
		Station						Station						Station					
		1	2	3	4	5	6	1	2	3	4	5	6	1	2	3	4	5	6
Radial outlet manifold (ROM-2); orifice																			
51	996	3 093	3 000	3 093	3 185	3 167	3 167	26	3	26	73	----	74	122	191	122	77	----	96
52	995	6 044	5 840	6 062	6 209	6 155	6 173	52	6	50	140	----	146	194	361	161	104	----	159
53	994	8 633	8 356	8 615	8 836	8 763	8 818	73	8	73	204	----	208	327	539	345	255	----	277
54	991	14 850	14 350	14 780	15 150	15 050	15 170	125	14	125	357	----	357	525	914	599	471	----	443
55	988	27 810	26 960	27 630	28 420	28 160	28 370	232	25	231	657	----	660	913	1556	1097	728	----	786
56	987	33 890	32 690	33 730	34 650	34 300	34 630	283	31	284	804	----	796	1193	2142	1360	956	----	965
Radial outlet manifold (ROM-2); orifice																			
268	988	1 249	1 157	1 249	1 323	1 378	1 323	23	2	23	66	----	66	163	235	162	132	----	132
269	987	2 661	2 476	2 680	2 827	2 920	2 780	50	6	51	146	----	144	366	506	349	296	----	331
270	986	7 077	6 576	7 077	7 465	7 761	7 447	136	15	138	398	----	400	1030	1408	1032	904	----	924
271	985	13 690	12 480	13 650	14 430	14 940	14 260	254	28	259	751	----	751	1891	2867	1933	1648	----	1815
272	985	29 200	26 700	29 250	30 680	31 910	30 750	545	60	558	1612	----	1612	4108	6118	4066	3697	----	3622
Radial outlet manifold (ROM-2); orifice																			
89	996	684	647	721	776	813	776	21	2	21	60	----	62	167	185	130	114	----	116
90	995	1 584	1 529	1 658	1 787	1 880	1 769	49	5	49	139	----	145	401	412	327	288	----	312
91	994	3 282	3 023	3 356	3 596	3 800	3 596	100	11	101	297	----	298	738	908	665	621	----	622
92	993	4 914	4 526	4 988	5 413	5 691	5 376	146	16	147	436	----	436	1095	1353	1022	886	----	923
93	990	6 710	6 377	6 987	7 487	7 875	7 505	202	22	206	603	----	602	1643	1796	1370	1267	----	1248
94	988	13 550	12 970	14 160	15 050	15 860	15 120	397	43	404	1200	----	1192	3179	3398	2576	2484	----	2402
95	986	21 100	20 270	21 670	23 320	24 780	23 500	622	67	637	1891	----	1871	5184	5461	4626	4235	----	4029
96	985	29 880	28 200	30 440	33 030	34 900	32 860	864	93	888	2641	----	2605	7152	8065	6621	5787	----	5916
97	983	2 920	2 772	3 012	3 253	3 419	3 271	87	9	88	263	----	260	737	807	646	580	----	559
Radial outlet manifold (ROM-2); orifice																			
230	994	670	615	670	762	799	762	33	3	32	98	----	99	218	243	217	191	----	192
231	992	1 339	1 228	1 321	1 520	1 616	1 520	65	7	64	196	----	198	452	505	469	402	----	404
232	990	2 534	2 294	2 534	2 867	3 089	2 867	123	13	123	377	----	378	864	994	864	785	----	786
233	989	4 290	3 902	4 235	4 808	5 159	4 826	204	21	203	622	----	625	----	----	----	----	----	----
234	988	5 900	5 327	5 863	6 658	7 102	6 658	281	29	280	862	----	866	----	----	----	----	----	----
235	987	8 787	7 844	8 732	9 794	10 488	9 855	414	43	415	1275	----	1281	----	----	----	----	----	----
236	986	15 360	13 800	15 160	16 900	18 240	16 960	714	75	717	2211	----	2225	4745	5663	4951	4703	----	4663
Radial outlet manifold (ROM-2); orifice																			
273	992	344	289	344	399	436	418	25	2	25	76	----	75	168	201	168	163	----	144
274	991	778	686	778	926	1 000	926	53	5	54	169	----	167	297	341	298	265	----	263
275	990	1 593	1 316	1 556	1 870	2 055	1 870	109	11	109	345	----	344	657	836	694	616	----	615
276	989	2 715	2 290	2 678	3 177	3 473	3 214	188	19	189	598	----	597	1198	1454	1236	1146	----	1108
277	988	4 254	3 699	4 199	4 938	5 382	4 994	290	30	293	925	----	921	1890	2185	1948	1841	----	1781
278	987	8 257	7 555	8 498	9 996	10 883	10 070	570	58	578	1830	----	1822	3691	4381	3958	3712	----	3630

manifolds

Reference velocity head at station a, $P_a - p_a$, N/m^2	Theoretical mass flow rate at orifice number, W_t, kg/sec						Reference velocity at station a, V_a, m/sec	Measured mass flow rate at orifice number, W_j, kg/sec						Reynolds number at reference station a, Re, dimensionless	Run
	Station							Station							
	1	2	3	4	5	6		1	2	3	4	5	6		
B; diameter, 1.91 cm; area, 2.854 cm^2															
105	0.706	0.695	0.706	0.716	0.714	0.714	0.460	0.446	0.445	0.445	0.454	0.449	0.460	35.3×10^3	51
204	.987	.970	.990	1.000	.986	.998	.640	.628	.625	.616	.624	.620	.639	55.8	52
293	1.179	1.160	1.178	1.193	1.188	1.191	.768	.744	.745	.743	.754	.744	.770	69.5	53
511	1.549	1.521	1.540	1.564	1.558	1.564	1.015	.976	.977	.974	1.008	.975	1.011	102	54
942	2.117	2.083	2.111	2.141	2.130	2.139	1.381	1.338	1.314	1.335	1.365	1.325	1.368	157	55
1151	2.338	2.296	2.332	2.363	2.351	2.353	1.527	1.474	1.456	1.478	1.510	1.460	1.501	182	56
C; diameter, 2.28 cm; area, 4.100 cm^2															
95	0.644	0.620	0.644	0.644	0.677	0.664	0.439	0.429	0.392	0.425	0.443	0.427	0.439	49.4×10^3	268
209	.941	.907	.944	.970	.986	.962	.651	.621	.613	.626	.652	.621	.645	76.9	269
572	1.534	1.479	1.534	1.576	1.606	1.574	1.077	1.022	1.017	1.032	1.074	1.025	1.090	131	270
1078	2.133	2.038	2.131	2.191	2.231	2.179	1.479	1.401	1.377	1.420	1.480	1.404	1.499	184	271
2319	3.116	2.981	3.120	3.196	3.260	3.200	2.170	2.046	2.019	2.083	2.165	2.052	2.201	277	272
D; diameter, 2.54 cm; area, 5.077 cm^2															
88	0.590	0.594	0.606	0.629	0.644	0.629	0.421	0.400	0.400	0.404	0.421	0.410	0.430	31.2×10^3	89
206	.899	.883	.919	.954	.979	.949	.643	.612	.607	.616	.647	.623	.663	52.3	90
424	1.293	1.241	1.306	1.352	1.391	1.354	.924	.875	.865	.884	.940	.894	.953	81.2	91
622	1.582	1.517	1.593	1.660	1.701	1.654	1.119	1.062	1.036	1.071	1.143	1.082	1.153	103	92
863	1.848	1.801	1.885	1.952	2.003	1.955	1.320	1.249	1.226	1.265	1.338	1.275	1.349	139	93
1718	2.630	2.570	2.686	2.771	2.843	2.777	1.865	1.753	1.711	1.778	1.902	1.791	1.913	214	94
2710	3.281	3.213	3.327	3.448	3.557	3.462	2.344	2.195	2.140	2.234	2.392	2.251	2.400	284	95
3774	3.903	3.782	3.938	4.103	4.218	4.096	2.768	2.586	2.523	2.639	2.832	2.649	2.838	354	96
376	1.219	1.187	1.238	1.286	1.319	1.290	.875	.822	.799	.831	.891	.838	.890	118	97
E; diameter, 2.86 cm; area, 6.415 cm^2															
141	0.738	0.708	0.738	0.788	0.810	0.788	0.533	0.505	0.488	0.499	0.555	0.525	0.553	47.2×10^3	230
283	1.044	1.000	1.037	1.112	1.146	1.112	.756	.712	.683	.704	.787	.740	.788	74.4	231
544	1.430	1.366	1.436	1.528	1.585	1.528	1.048	.984	.942	.979	1.094	1.027	1.092	112	232
901	1.867	1.781	1.855	1.978	2.050	1.982	1.350	1.264	1.211	1.261	1.399	1.319	1.405	149	233
1246	2.190	2.081	2.183	2.328	2.404	2.328	1.588	1.490	1.414	1.484	1.653	1.551	1.657	179	234
1848	2.672	2.528	2.667	2.841	2.920	2.832	1.935	1.804	1.720	1.806	2.010	1.894	2.022	227	235
3209	3.538	3.352	3.512	3.710	3.855	3.717	2.551	2.367	1.262	2.375	2.651	2.486	2.678	310	236
F; diameter, 3.18 cm; area, 7.917 cm^2															
110	0.653	0.598	0.653	0.704	0.736	0.720	0.471	0.445	0.413	0.444	0.494	0.475	0.483	46.4×10^3	273
246	.982	.922	.982	1.072	1.113	1.072	.704	.651	.611	.654	.743	.713	.736	71.6	274
502	1.405	1.276	1.388	1.523	1.596	1.523	1.007	.932	.871	.933	1.065	1.013	1.060	107	275
872	1.834	1.685	1.820	1.984	2.073	1.995	1.328	1.226	1.143	1.227	1.403	1.336	1.401	147	276
1350	2.297	2.140	2.280	2.470	2.582	2.488	1.653	1.519	1.424	1.528	1.743	1.660	1.742	190	277
2671	3.295	3.060	3.245	3.250	3.674	3.535	2.326	2.128	1.996	2.151	2.453	2.334	2.463	272	278

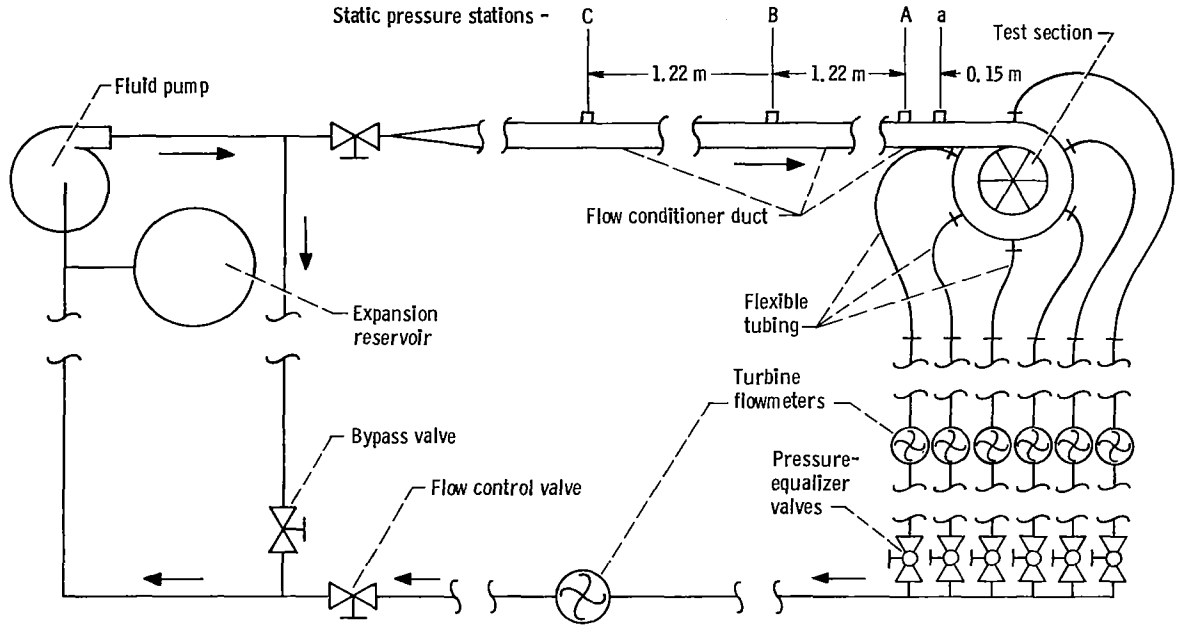

(a) Arrangement for inlet manifold tests.

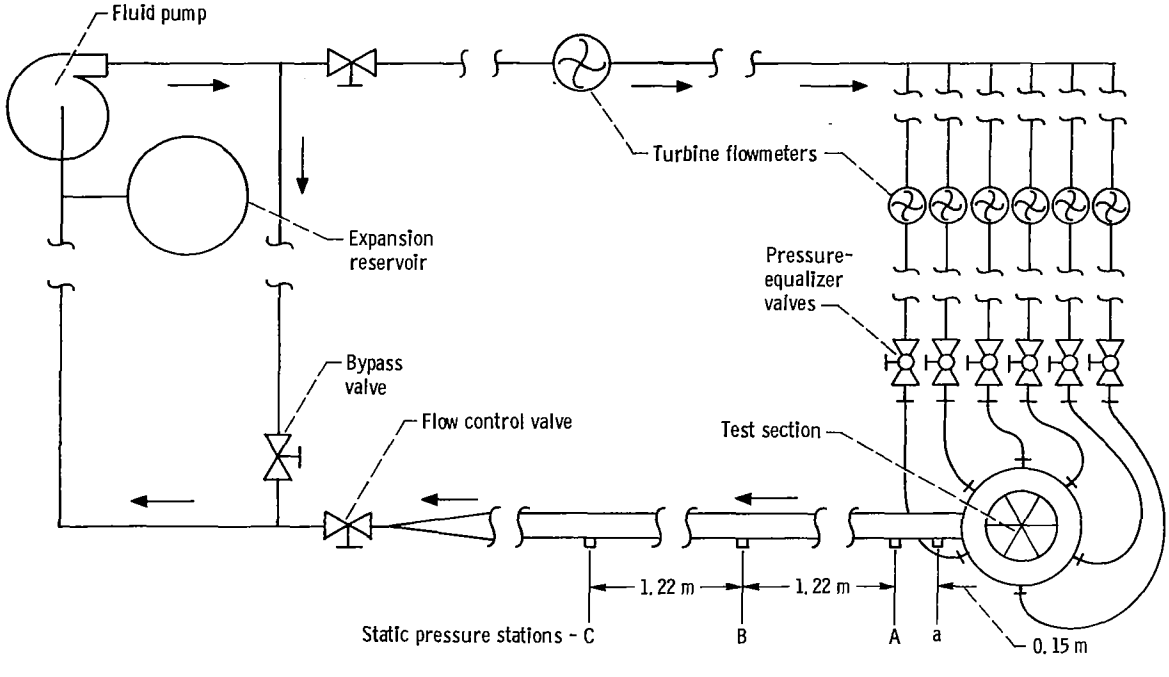

(b) Arrangement for outlet manifold tests.

Figure 1. - Schematic diagram of recirculating test loop.

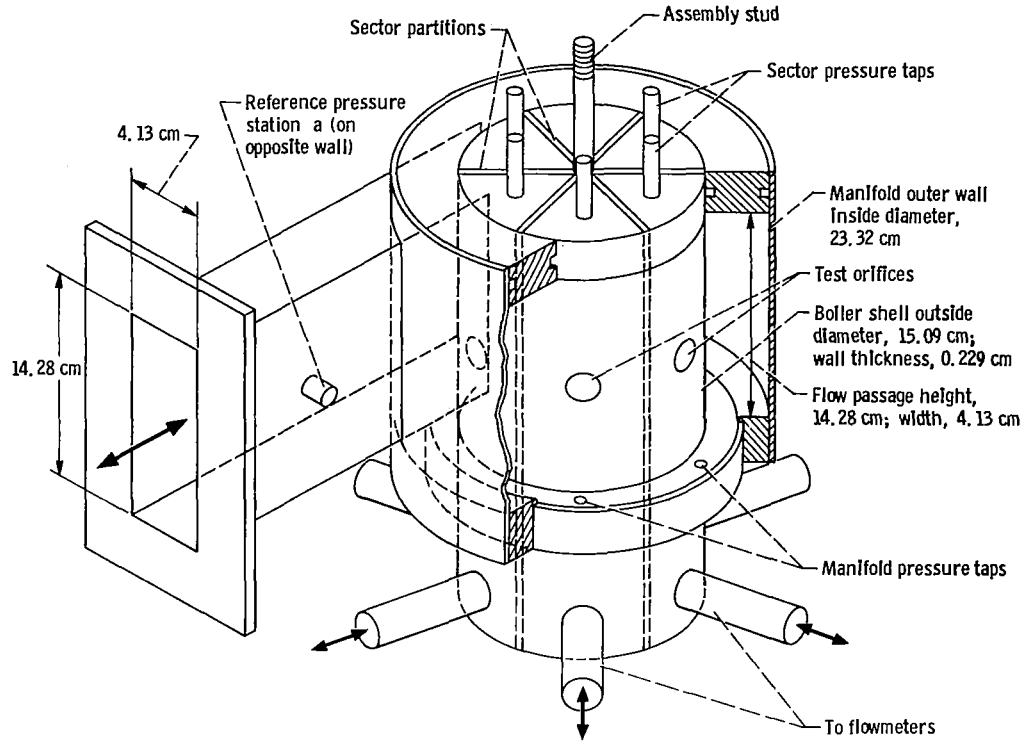

(a) With tangential manifold.

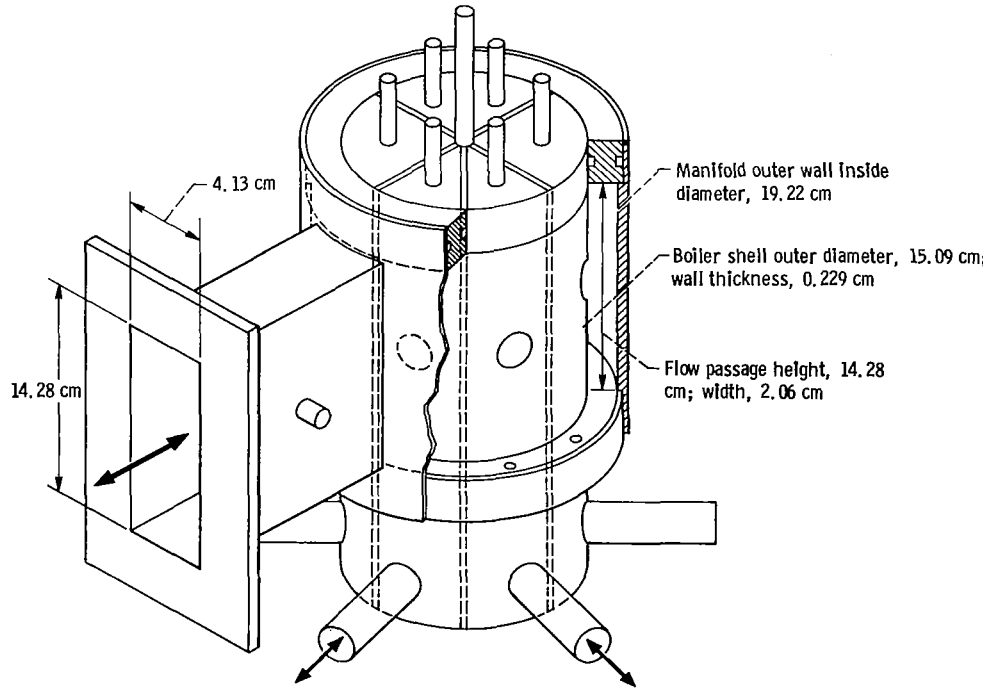

(b) With radial manifold.

Figure 2. - Details of simulated boiler shell and manifold.

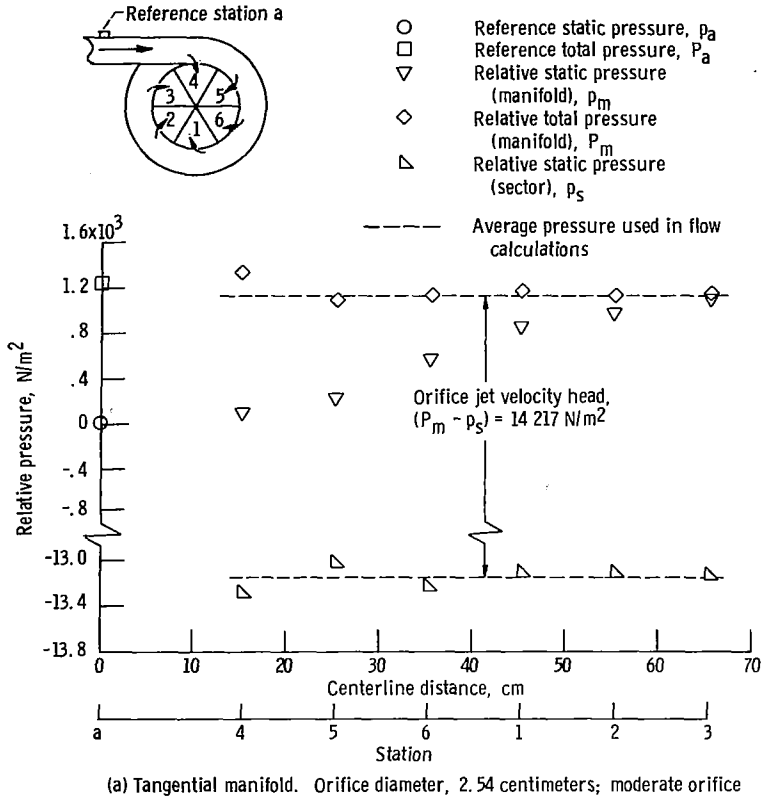

(a) Tangential manifold. Orifice diameter, 2.54 centimeters; moderate orifice pressure drop.

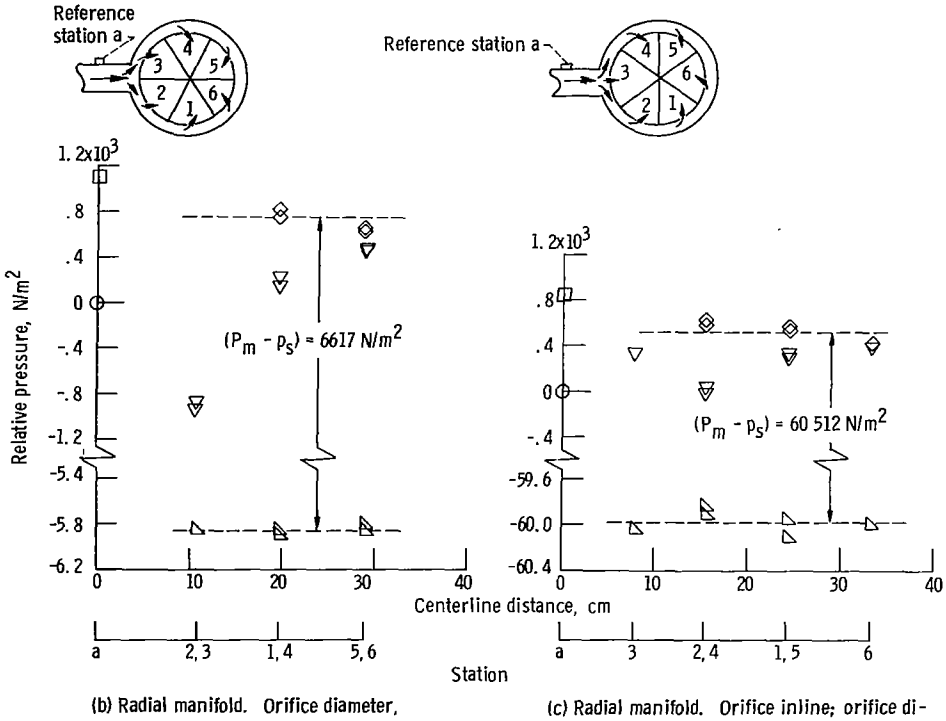

(b) Radial manifold. Orifice diameter, 3.18 centimeters; low orifice pressure drop.

(c) Radial manifold. Orifice inline; orifice diameter, 1.59 centimeters; high pressure drop.

Figure 3. - Typical inlet manifold pressure map

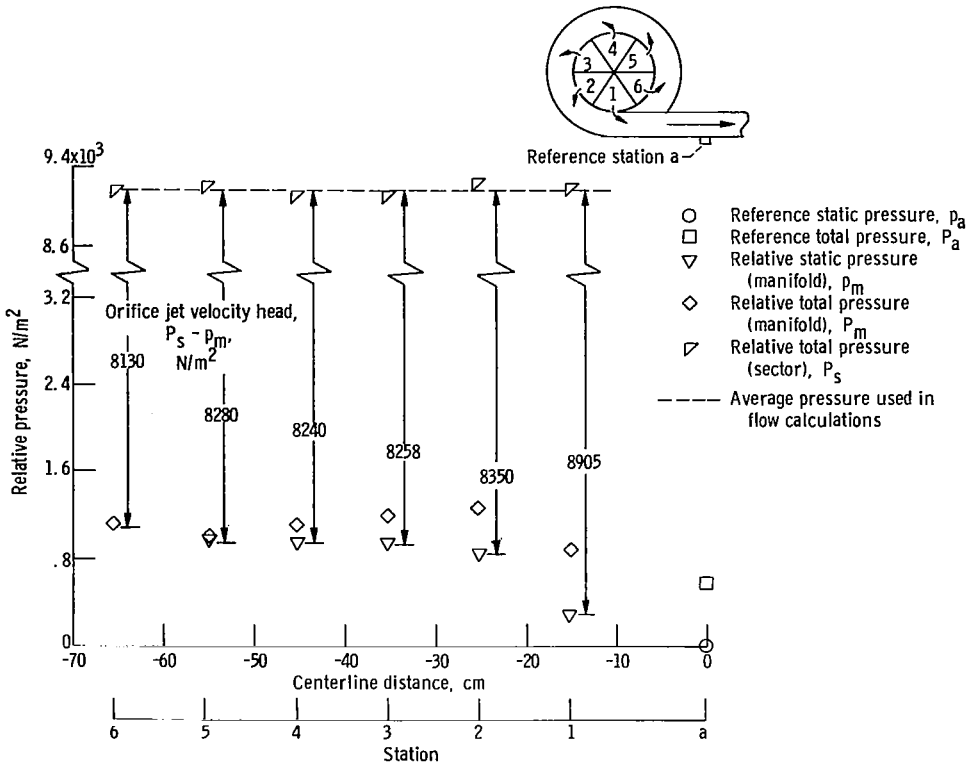

(a) Tangential manifold. Orifice diameter, 2.28 centimeters; moderate orifice pressure drop.

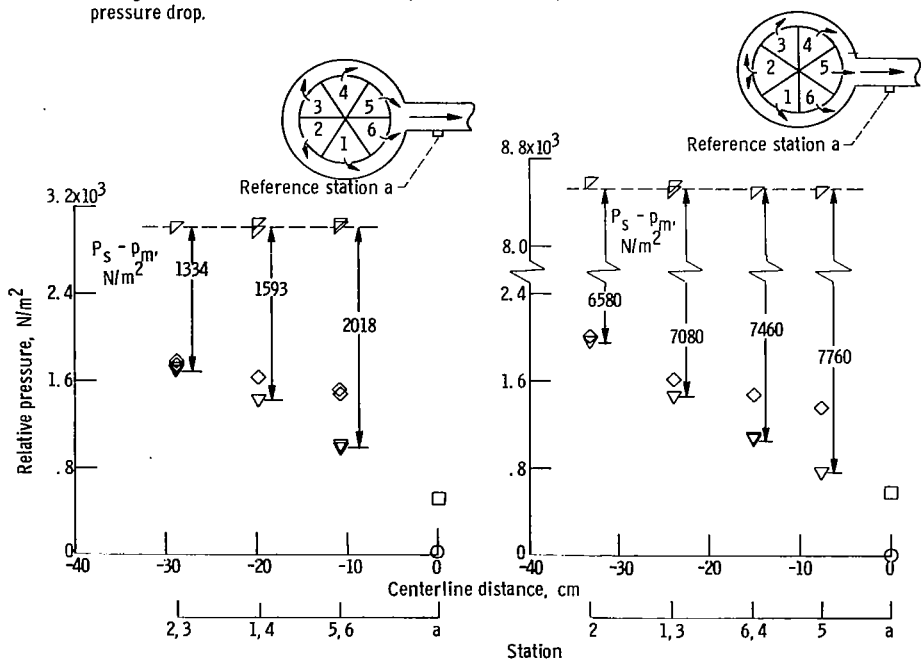

(b) Radial manifold. Orifice diameter, 3.18 centimeters; low orifice pressure drop.

(c) Radial manifold. Orifice inline, orifice diameter, 2.28 centimeters; moderate orifice pressure drop.

Figure 4. - Typical outlet manifold pressure map.

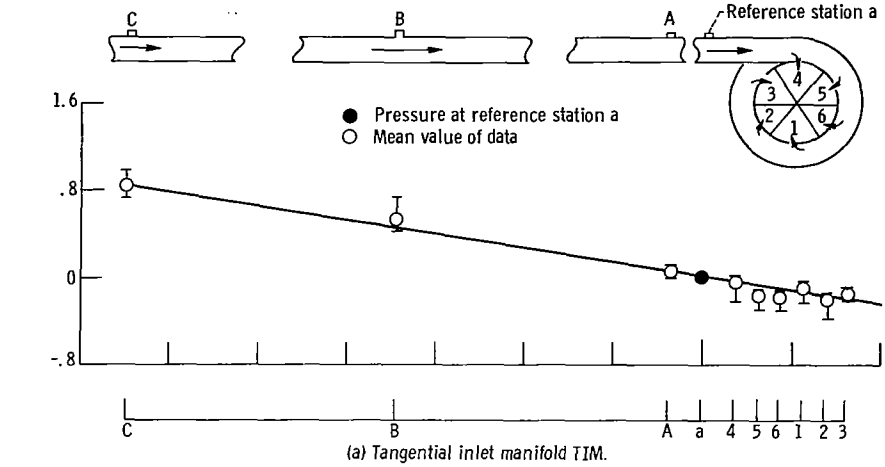

(a) Tangential inlet manifold TIM.

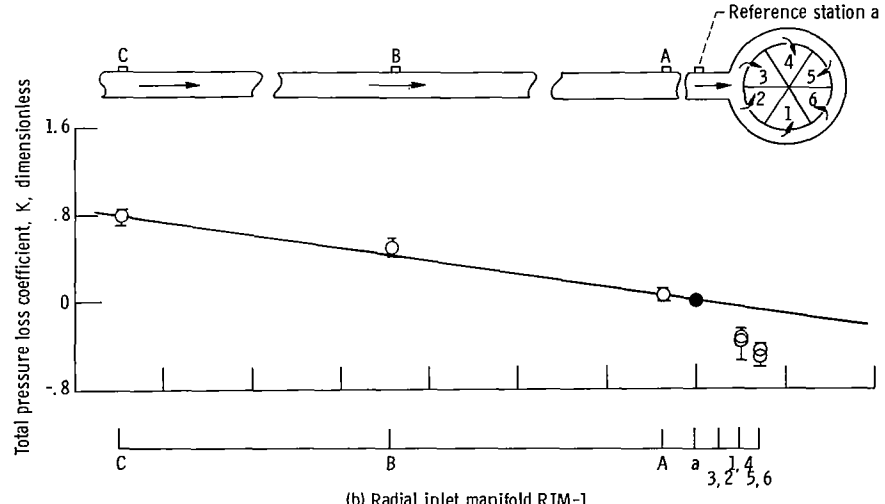

(b) Radial inlet manifold RIM-1.

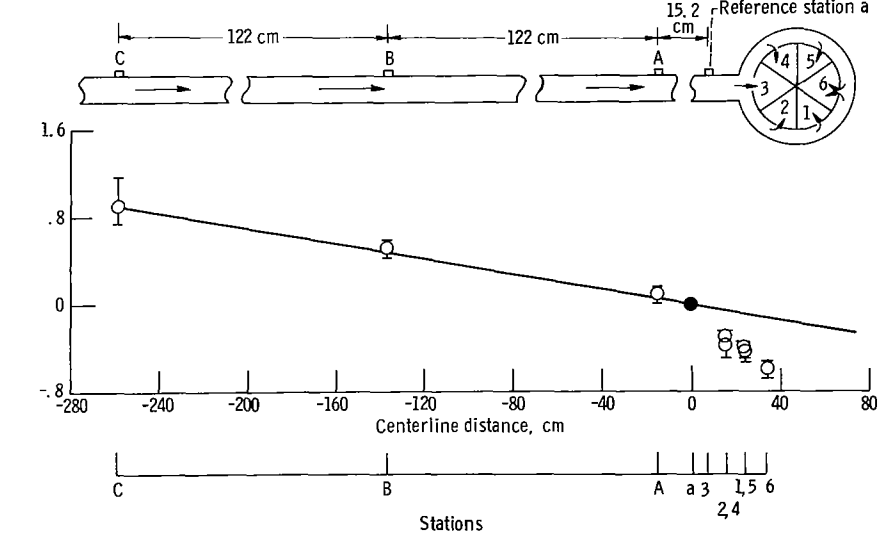

(c) Radial inlet manifold RIM-2.

Figure 5. - Total pressure loss coefficient plotted as function of duct and manifold centerline distance from reference station a. Orifice diameter, 1.59 centimeters.

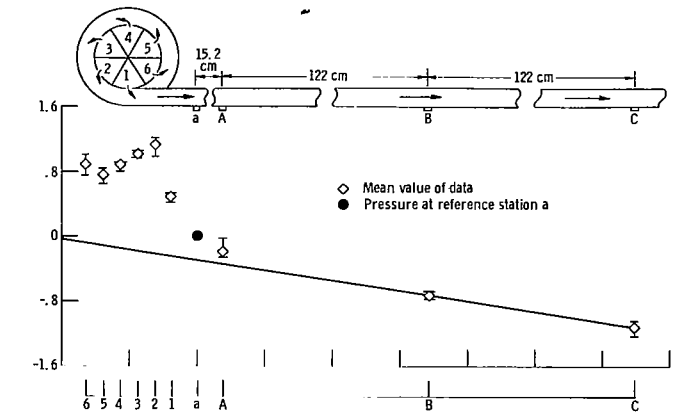

(a) Tangential outlet manifold TOM.

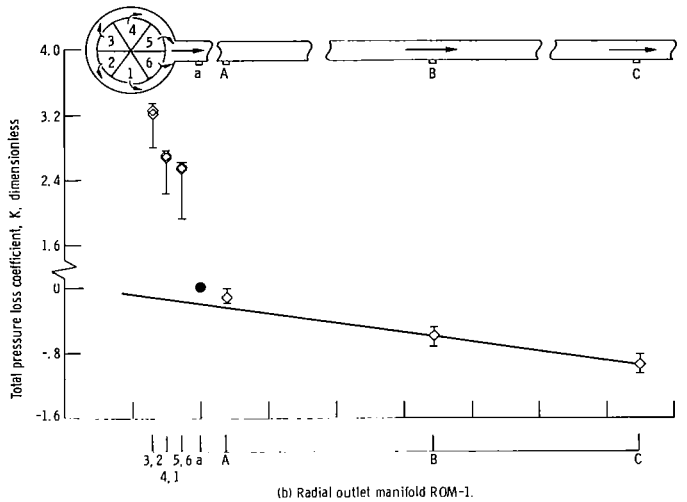

(b) Radial outlet manifold ROM-1.

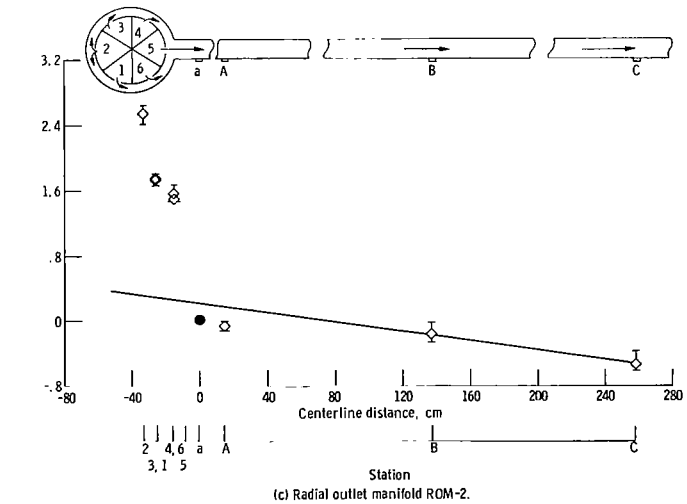

(c) Radial outlet manifold ROM-2.

Figure 6. - Total pressure loss coefficient plotted as function of duct and manifold centerline distance from reference station a. Orifice diameter, 2.28 centimeters.

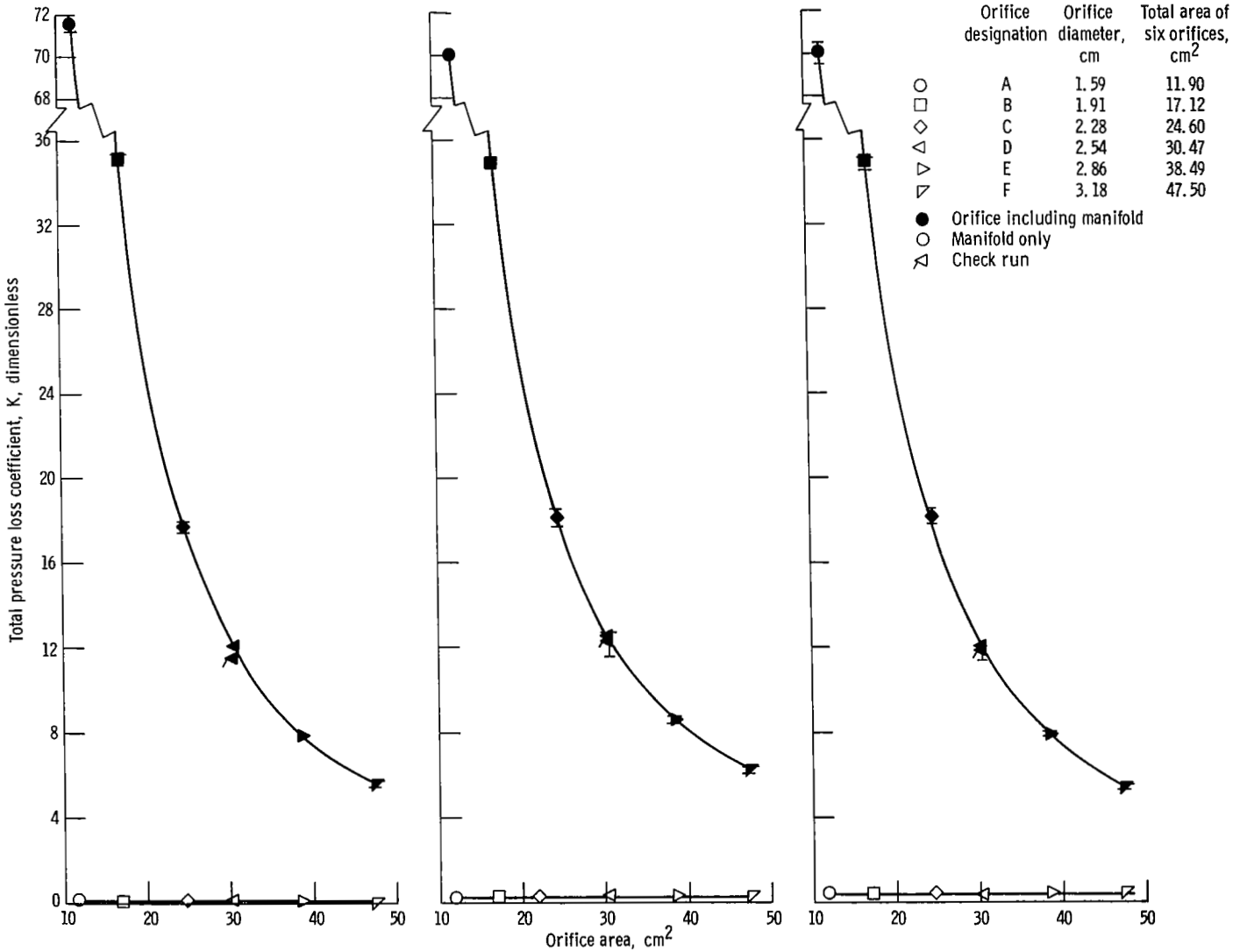

(a) Tangential inlet manifold TIM. (b) Radial inlet manifold RIM-1. (c) Radial inlet manifold RIM-2.

Figure 7. - Effect of orifice total area on orifice and manifold pressure loss coefficients K with inlet manifolds.

	Orifice designation	Orifice diameter, cm	Total area of six orifices, cm^2
□	B	1.91	17.12
◇	C	2.28	24.60
◁	D	2.54	30.47
▷	E	2.86	38.49
▽	F	3.18	47.50

Solid symbols denote orifices including manifold
Open symbols denote manifold only

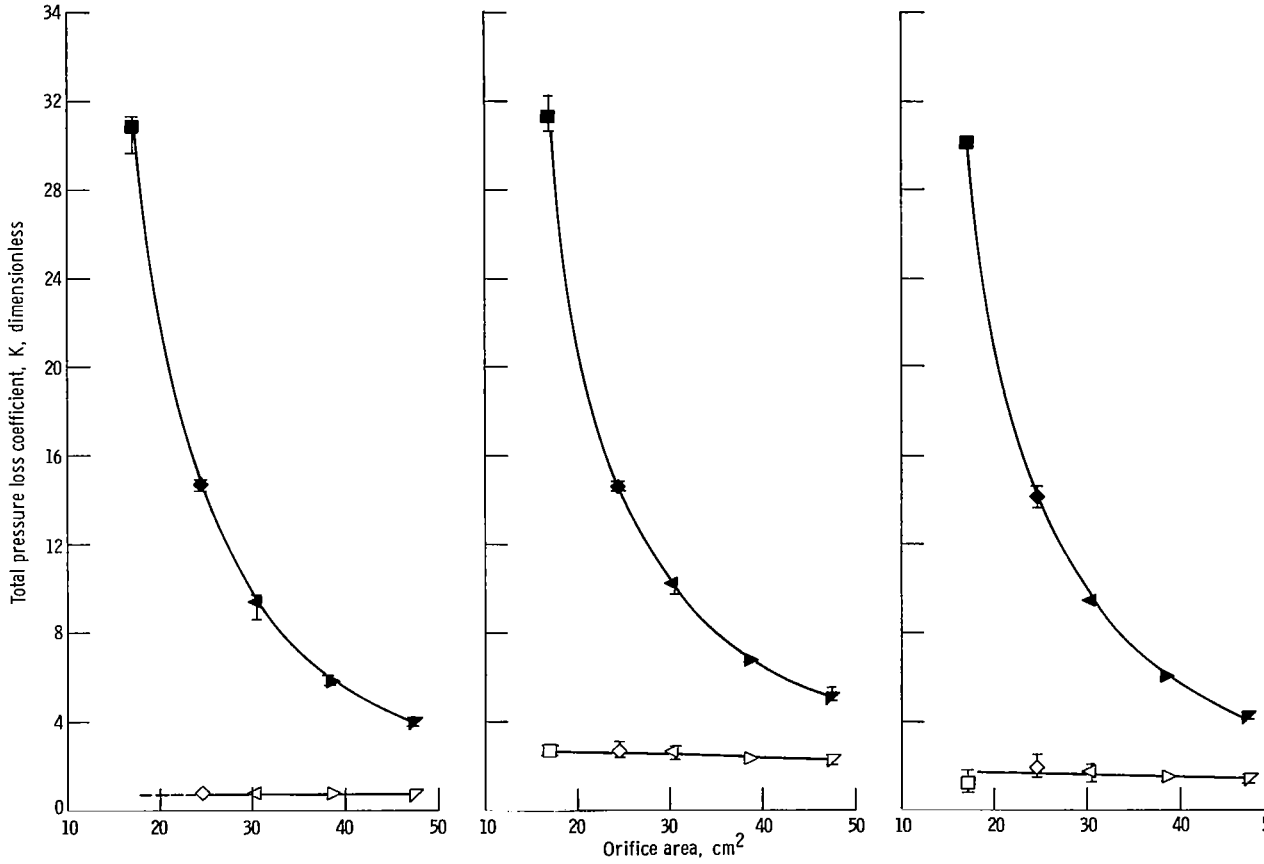

(a) Tangential outlet manifold TOM.

(b) Radial outlet manifold ROM-1.

(c) Radial outlet manifold ROM-2.

Figure 8. - Effect of orifice total area on orifice and manifold pressure loss coefficients K with outlet manifolds.

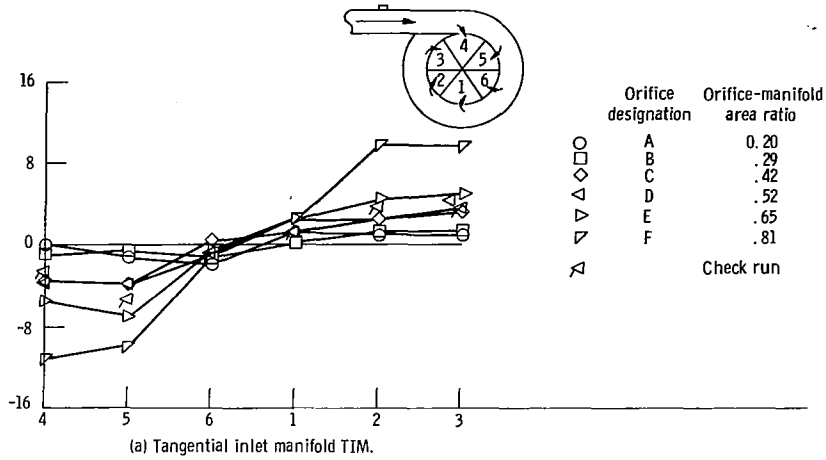

(a) Tangential inlet manifold TIM.

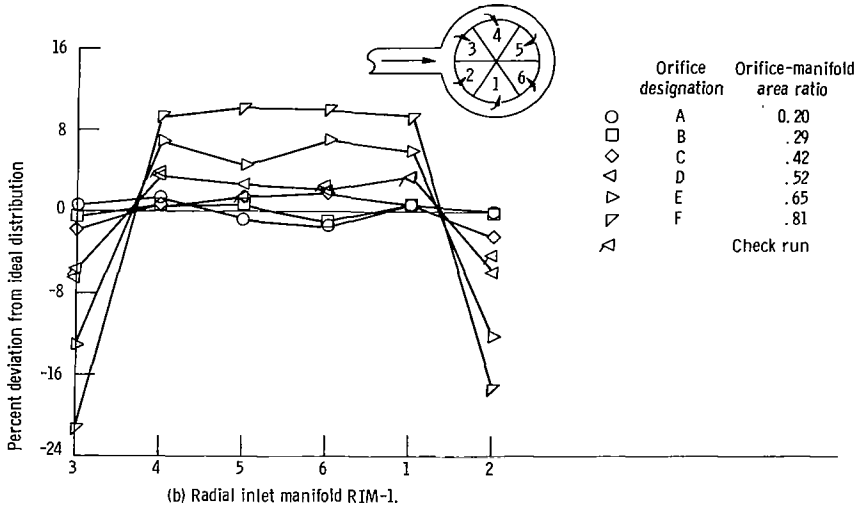

(b) Radial inlet manifold RIM-1.

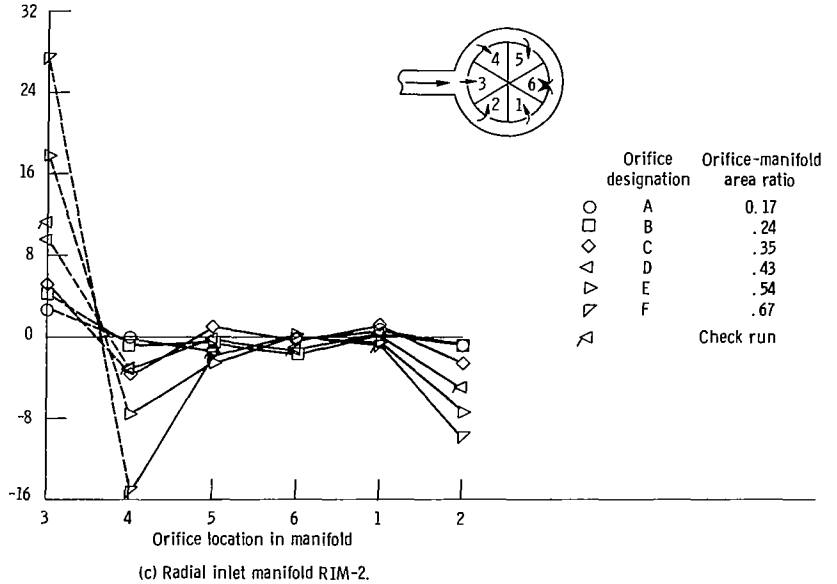

(c) Radial inlet manifold RIM-2.

Figure 9. - Percent deviation from ideal distribution for six orifice sizes with inlet manifolds.

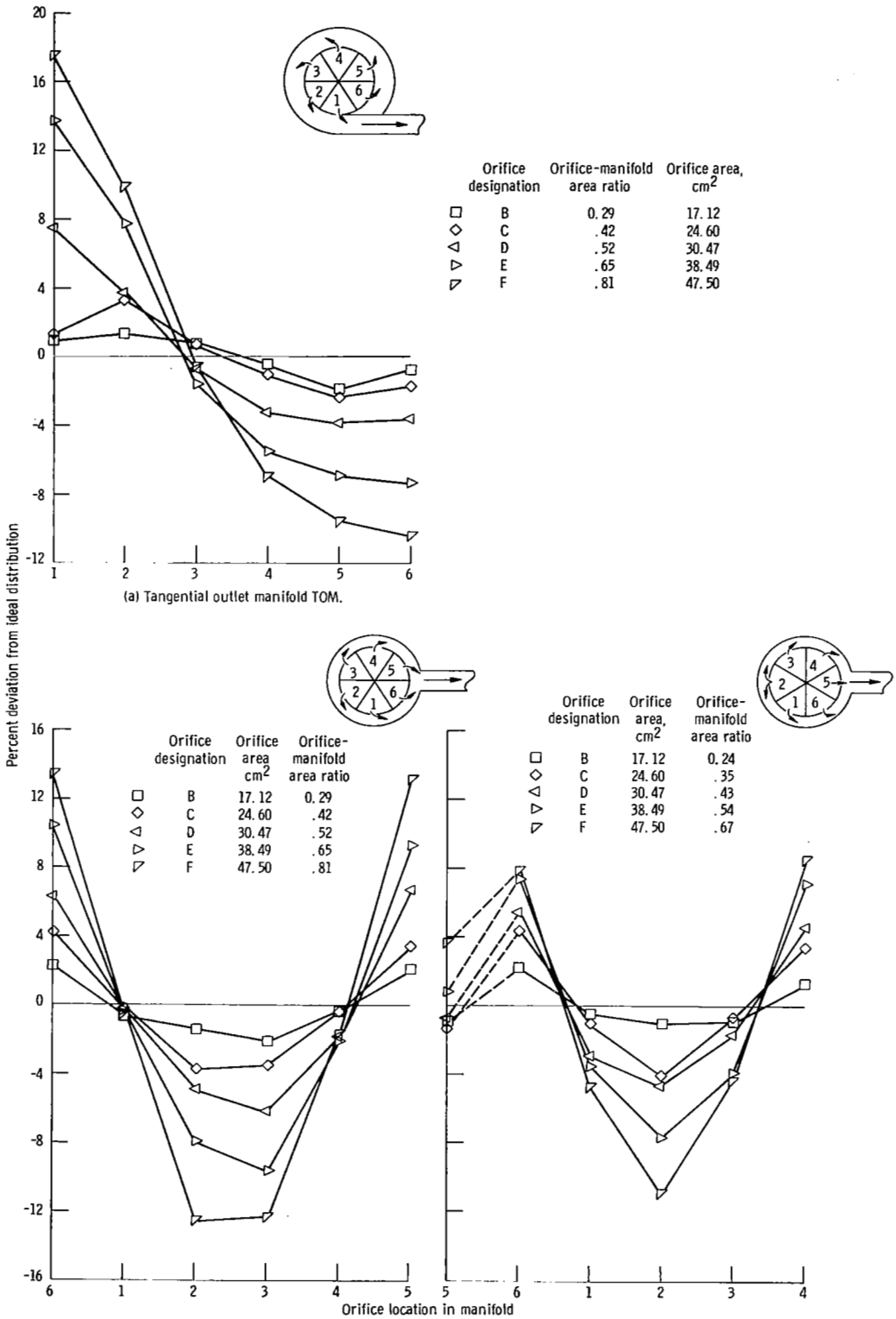

(a) Tangential outlet manifold TOM.

(b) Radial outlet manifold ROM-1.

(c) Radial outlet manifold ROM-2.

Figure 10. - Percent deviation from ideal distribution for five orifice sizes with outlet manifolds.

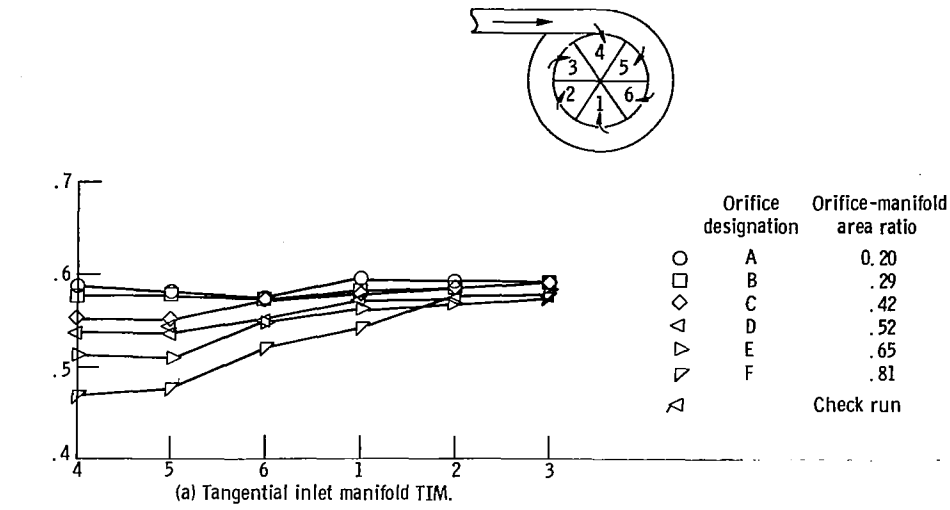

(a) Tangential inlet manifold TIM.

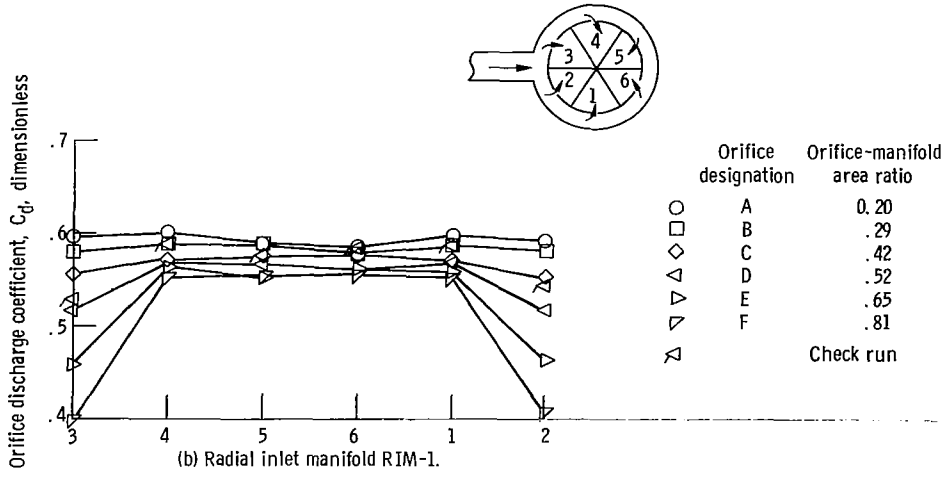

(b) Radial inlet manifold RIM-1.

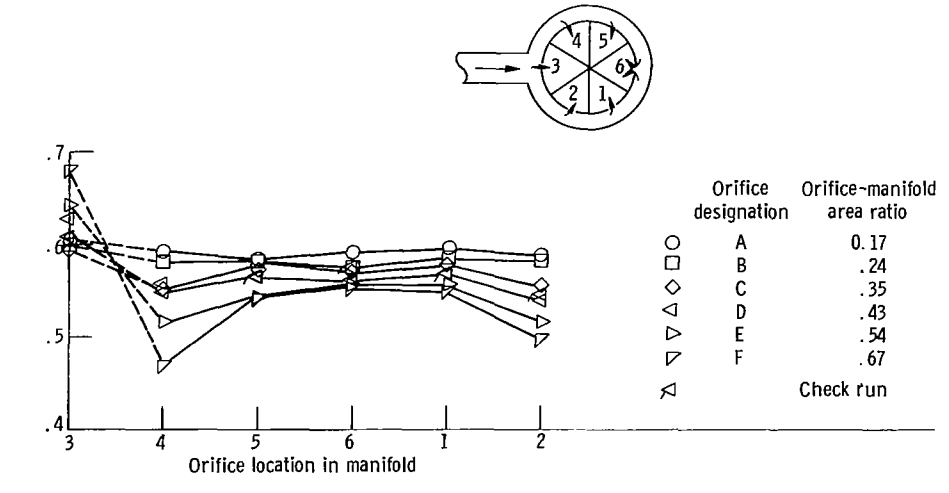

(c) Radial inlet manifold RIM.

Figure 11. - Variation in orifice discharge coefficient with location in inlet manifold.

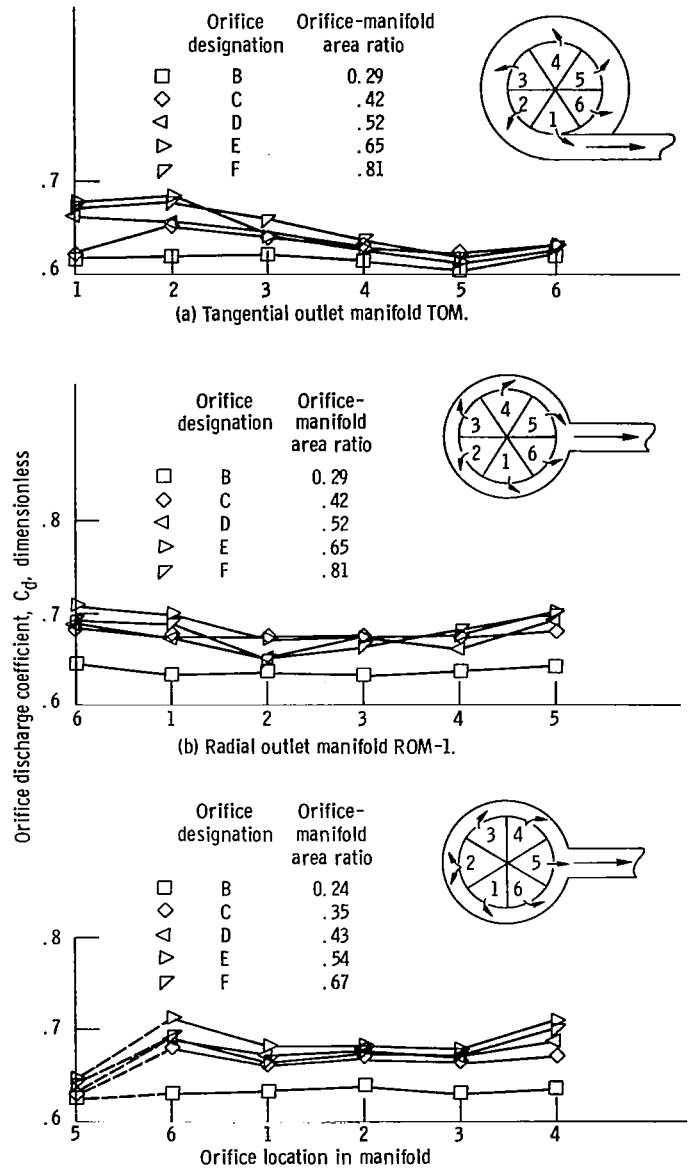

Figure 12. - Variation in orifice discharge coefficient with location in outlet manifold.

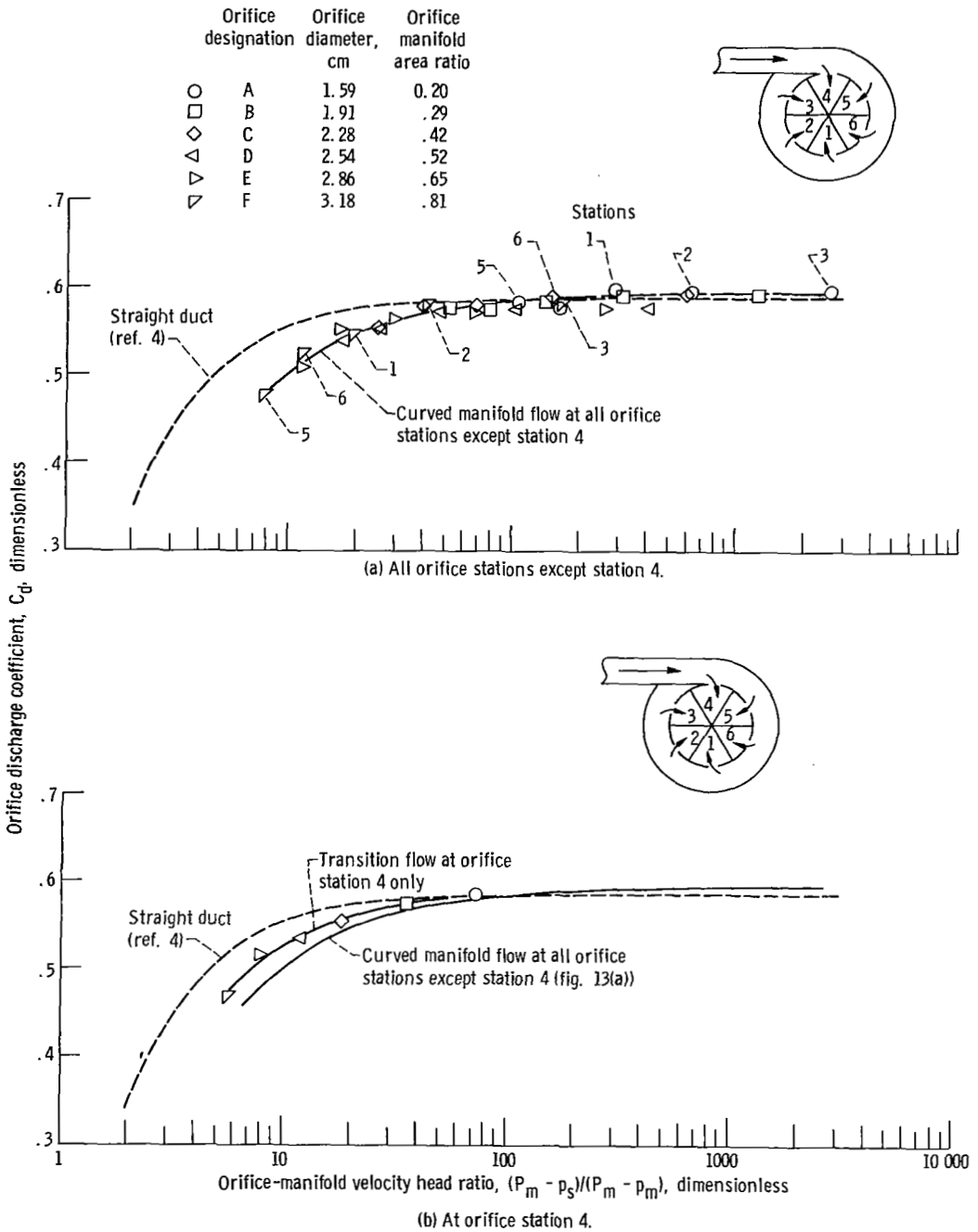

Figure 13. - Variation of orifice discharge coefficient with orifice-manifold velocity head ratio for tangential inlet manifold TIM.

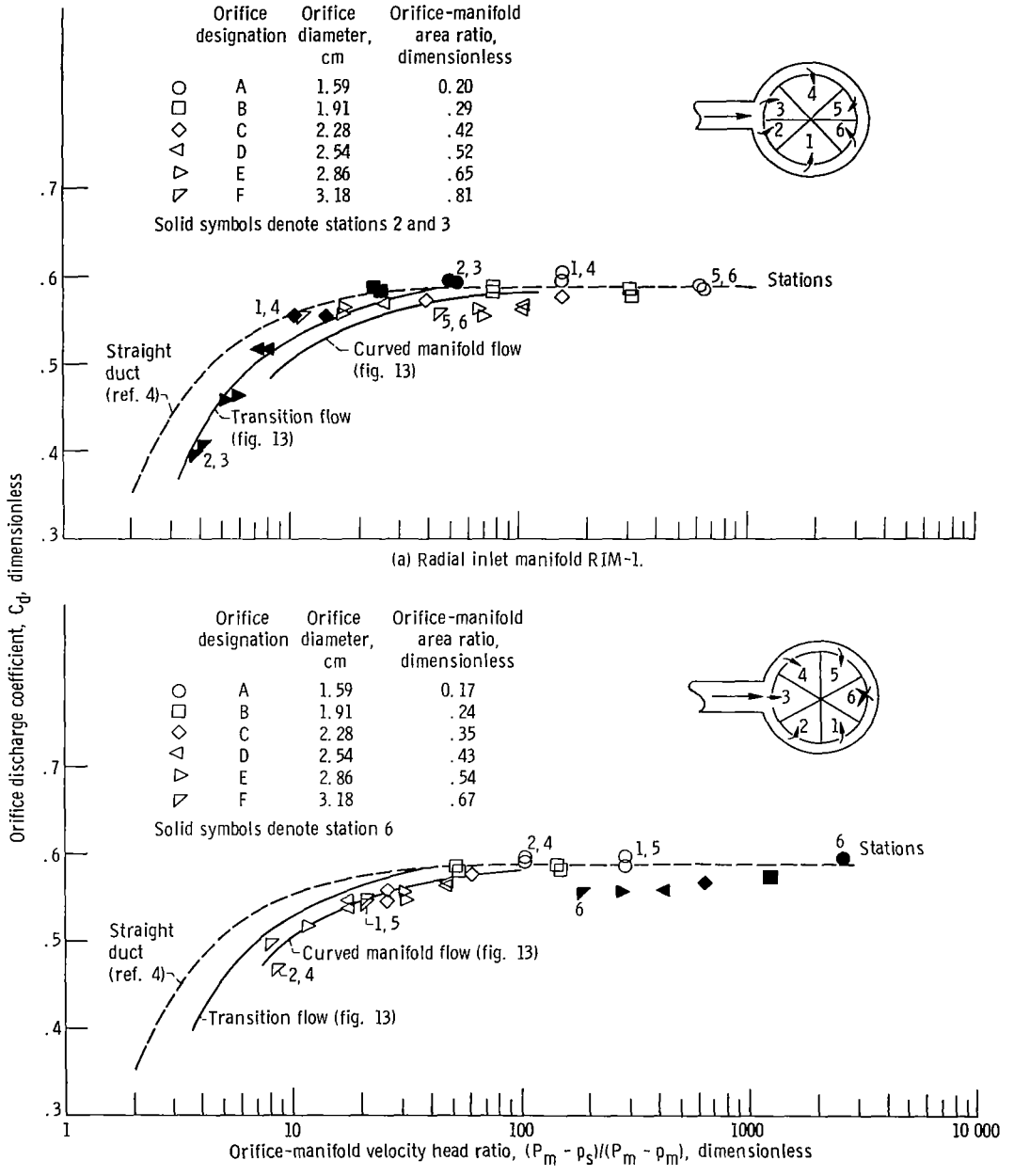

Figure 14. - Variation of orifice discharge coefficient with orifice-manifold velocity head ratio.

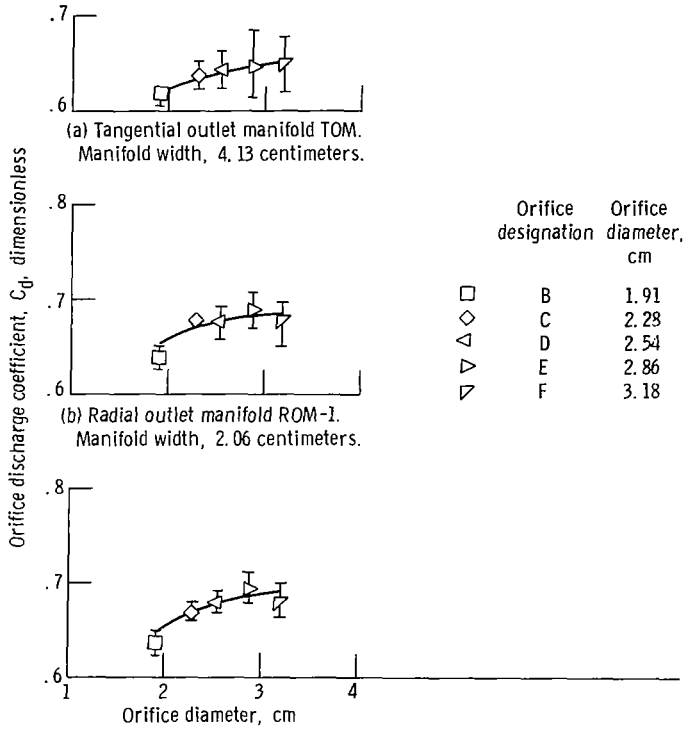

Figure 15. - Variation of orifice discharge coefficient with orifice diameter for orifices in circumferential outlet manifolds having a 14.6-centimeter inside diameter.

NASA-Langley, 1972 — 33 E-6619

"The aeronautical and space activities of the United States shall be conducted so as to contribute . . . to the expansion of human knowledge of phenomena in the atmosphere and space. The Administration shall provide for the widest practicable and appropriate dissemination of information concerning its activities and the results thereof."

—NATIONAL AERONAUTICS AND SPACE ACT OF 1958

NASA SCIENTIFIC AND TECHNICAL PUBLICATIONS

TECHNICAL REPORTS: Scientific and technical information considered important, complete, and a lasting contribution to existing knowledge.

TECHNICAL NOTES: Information less broad in scope but nevertheless of importance as a contribution to existing knowledge.

TECHNICAL MEMORANDUMS: Information receiving limited distribution because of preliminary data, security classification, or other reasons.

CONTRACTOR REPORTS: Scientific and technical information generated under a NASA contract or grant and considered an important contribution to existing knowledge.

TECHNICAL TRANSLATIONS: Information published in a foreign language considered to merit NASA distribution in English.

SPECIAL PUBLICATIONS: Information derived from or of value to NASA activities. Publications include conference proceedings, monographs, data compilations, handbooks, sourcebooks, and special bibliographies.

TECHNOLOGY UTILIZATION PUBLICATIONS: Information on technology used by NASA that may be of particular interest in commercial and other non-aerospace applications. Publications include Tech Briefs, Technology Utilization Reports and Technology Surveys.

Details on the availability of these publications may be obtained from:

SCIENTIFIC AND TECHNICAL INFORMATION OFFICE

NATIONAL AERONAUTICS AND SPACE ADMINISTRATION

Washington, D.C. 20546